

PNNL-33587

Fragility Functions Resource Report

Documented Sources for Electricity
and Water Resilience Valuation

October 2022

Wilfried Kabre
Mark R. Weimar

DISCLAIMER

This report was prepared as an account of work sponsored by an agency of the United States Government. Neither the United States Government nor any agency thereof, nor Battelle Memorial Institute, nor any of their employees, makes **any warranty, express or implied, or assumes any legal liability or responsibility for the accuracy, completeness, or usefulness of any information, apparatus, product, or process disclosed, or represents that its use would not infringe privately owned rights.** Reference herein to any specific commercial product, process, or service by trade name, trademark, manufacturer, or otherwise does not necessarily constitute or imply its endorsement, recommendation, or favoring by the United States Government or any agency thereof, or Battelle Memorial Institute. The views and opinions of authors expressed herein do not necessarily state or reflect those of the United States Government or any agency thereof.

PACIFIC NORTHWEST NATIONAL LABORATORY
operated by
BATTELLE
for the
UNITED STATES DEPARTMENT OF ENERGY
under Contract DE-AC05-76RL01830

Printed in the United States of America

Available to DOE and DOE contractors from the
Office of Scientific and Technical Information,
P.O. Box 62, Oak Ridge, TN 37831-0062;
ph: (865) 576-8401
fax: (865) 576-5728
email: reports@adonis.osti.gov

Available to the public from the National Technical Information Service
5301 Shawnee Rd., Alexandria, VA 22312
ph: (800) 553-NTIS (6847)
email: orders@ntis.gov <<https://www.ntis.gov/about>>
Online ordering: <http://www.ntis.gov>

Fragility Functions Resource Report

Documented Sources for Electricity and Water Resilience Valuation

October 2022

Wilfried Kabre
Mark R. Weimar

Prepared for
the U.S. Department of Energy
under Contract DE-AC05-76RL01830

Pacific Northwest National Laboratory
Richland, Washington 99354

Abstract

Fragility curves provide the vulnerability between hazard intensity and an asset. Federal installations may include many different electricity and water infrastructure types (or assets) such as generators, wind turbines, solar PV, switch yards, substations and power lines as well as water distribution systems that could be affected by different hazards. The vulnerability of each asset is a function of its age, type of materials and maintenance. In addition, the vulnerability changes with the hazards intensity and has a probability distribution function associated with it. The fragility functions are used in conjunction with hazard probability and consequence valuations to determine the values at risk for examination of investment grade analyses of alternative mitigation strategies. This document provides examples of fragility functions and links to their sources for different electricity and water infrastructure assets by hazard type.

Summary

Fragility curves provide the vulnerability between hazard intensity and an asset. Federal installations may include many different electricity and water infrastructure types (or assets) such as generators, wind turbines, solar PV, switch yards, substations and power lines as well as water distribution systems that could be affected by different hazards. The vulnerability of each asset is a function of its age, type of materials and maintenance. In addition, the vulnerability changes with the hazards intensity and has a probability distribution function associated with it. For example, a hazard like a hurricane and associated flooding, earthquake, or tornado doesn't come with one probability and the value of the damage comes with its own probability function. Thus, the value of the loss is not simply the probability of hazard times the probability of the vulnerability times the probability of the consequence as we usually do in a simple risk equation.

Thus, the fragility functions are used in conjunction with hazard probability and consequence valuations to determine the values at risk for examination of investment grade analyses of alternative mitigation strategies. The solution is more appropriately approached using a Monte Carlo simulation to draw from appropriate distribution functions for each hazard, vulnerability and consequence for each asset. If the analyst only uses the simple approach, the value at risk likely doesn't well represent the multivariate probability solution. Using the inappropriately defined value of risk could affect the benefit cost analysis in such a way as to choose a solution that provides benefit cost ratios (BCR) greater than 1 that reduce the risk faced by the installation, but not as much as a mitigation solution that if properly valued could reduce the risk substantially more but didn't provide a BCR greater than 1 using the simpler approach to evaluating the value at risk.

This paper provides examples of the fragility curves by hazard infrastructure system (electricity and water) and the associated asset type and documents and provides links to their sources for different electricity and water infrastructure assets by hazard type. The following hazards (Table E.1) were found to have fragility functions associated with different infrastructure types associated with energy and water delivery.

Table E.1. Hazards with electricity and water infrastructure fragility functions

Climate Based Hazards	Non-Climate Based Hazards
Tornado	Earthquakes
Hurricane	Volcano
Wildfire	Geomagnetic Storms
High Wind	
Flood	
Wind and Ice	
Tsunami	

The following are some of the assets found, documented and sourced: Substation, transmission and distribution, power generation plant, hydropower system, high voltage equipment, wind turbines, transformer, power grid, concrete pole, utility pole, circuit breaker, telecommunication tower, tower line, and a transmission tower.

Acknowledgments

We wish to thank the US Department of Energy Federal Energy Management Program for providing the funding and guidance in developing this resource.

Acronyms and Abbreviations

BCR	Benefit Cost Ratio
CLIP	Cascadia Lifelines Program
PGA	Point ground acceleration

Contents

Abstract.....	ii
Summary	iii
Acknowledgments.....	iv
Acronyms and Abbreviations.....	v
1.0 Introduction	1
2.0 Earthquakes	4
2.1 CLIP Lifelines Fragility Database	4
2.1.1 Content.....	4
2.1.2 How to use the database.....	5
2.2 Concrete distribution poles.....	5
2.3 Transformers	6
2.4 Electric Substation Equipment	8
2.5 High-Voltage Electrical Equipment.....	9
2.6 Electric Power Stations	10
2.7 Hydropower Systems.....	11
2.8 Power Grid.....	12
2.9 Wind Turbine	13
2.10 Lifelines	14
3.0 Wind.....	16
3.1 Wind Turbine	16
3.2 Wind Turbine	17
3.3 Utility Poles.....	18
3.4 Utility pole	19
3.5 Utility Pole.....	20
3.6 Circuit Breaker	21
3.7 Telecommunication Towers	22
3.8 Tower lines	23
3.9 Transmission lines	24
3.10 Communication Tower	25
3.11 Transmission Towers.....	26
3.12 Transmission Overhead Line	27
4.0 Hurricane.....	29
4.1 Transmission Tower Line	29
4.2 Transmission Towers.....	30
4.2.2 Transmission Tower	31
4.3 Solar Panel.....	32

4.4 Power Grid33

4.5 Electrical Conductors.....34

4.6 Energy Infrastructure35

4.7 Residential Buildings36

4.8 Nuclear Power Plant Piping37

4.9 Yucca Mountain Nuclear Waste Repository.....38

4.10 Electric Substations39

4.11 Urban Gas Pipelines.....40

4.12 Oil Pumping Station.....41

5.0 Ice Loads.....42

5.1 Transmission Towers.....42

6.0 Flood44

6.1 Buildings.....44

6.2 Electrical Component.....45

6.3 Electric Components46

6.4 Electrical Grid47

6.5 Power Grid48

7.0 Tsunami50

7.1 Utility Pole50

8.0 Volcanic.....51

8.1 Water Treatment Site.....51

9.0 Geomagnetic Storms.....53

9.1 Power Grid53

10.0 Heat54

10.1 Distribution Transformers54

11.0 Tornado.....55

11.1 School Building.....55

11.2 Residential Building56

12.0 Power Outage57

12.1 Manufacturing Plant.....57

12.2 Health Care58

12.3 Industrial Customers.....59

13.0 References.....60

Figures

Figure 1. Fragility curves for (a) the 9 m -long, (b) 12 m-long, and (c) 15 m-long poles.....6

Figure 2. Fragility curves for different damage states of the mold transformer.....8

Figure 3. Exceedance probability of 63KV post insulator, DI values of 11.72 MPa(left) and 23.44 MPa (right).9

Figure 4. Damage probability curves for all kinds of high voltage electrical equipment..... 10

Figure 5. Fragility curves for small generation plants, with anchored (left) and unanchored (right components). 11

Figure 6. Probability distributions for hydroelectric components at the selected site. (a) Slight damage, (b) light damage, (c) Moderate damage, (d) Heavy damage..... 12

Figure 7. Cumulative distribution function (capacity curves) for the transformer. 13

Figure 8. Fragility Curve for different damage states of the 5-MW NREL wind turbine for 2.5 m/s wind speed. 14

Figure 9. Empirical fragility curves for power grids made up of substations of different voltages based on data from US west coast earthquakes. 15

Figure 10. Fragility curves different size wind turbines: (A) 1 MW wind turbine, (B) 2.5 MW wind turbine, (C) 3.3 MW wind turbine. 17

Figure 11. Fragility curves for wind turbine blades in parked conditions. 18

Figure 12. Fragility curves of new wood and steel poles. 19

Figure 13. Wind fragility curves pole and 30 degree leaning pole showing that leaning can increase failure probability. 20

Figure 14. Example fragility curve for wind damage to utility poles..... 21

Figure 15. Fragility curve for transmission lines..... 22

Figure 16. Fragility curves for wind speed and ice thickness combinations. 23

Figure 17. Wind-related fragility curves of transmission lines and towers. 24

Figure 18. Fragility of transmission lines based on wind speed 25

Figure 19. Communication tower fragility due to wind speed..... 26

Figure 20. Profiles of normal wind and downburst with different jet diameters..... 27

Figure 21. OHL fragility curve used in the proposed study. 28

Figure 22. Fragility Curve Tower-line System based different wind angles and wind speed..... 29

Figure 23. Fragility curves for transmission towers under 90° wind direction..... 31

Figure 24. Wind fragility curve of a transmission tower..... 32

Figure 25. Fragility function for solar panels due to wind speed 33

Figure 26. Fragility curves for different types of power plants..... 34

Figure 27. Fragility curves for conductor based on wind speed with span length of 200,300,400, and 500 meters. 35

Figure 28. Fragility curves by technology based on wind speed..... 36

Figure 29. Fragility function for residential buildings based on wind speed..... 37

Figure 30. Seismic fragility curve for nuclear plant piping using the collapse load point as a failure criterion 38

Figure 31. Hypothetical fragility curves for individual and combined fragility for: (a) event sequence 3 and (b) event sequence 4. 39

Figure 32. Fragility functions for substations with anchored and unanchored components..... 39

Figure 33. Fragility curves for electric power lines according to failure levels to a seismic event.....40

Figure 34. Exclusive fragility curves and parameters for an oil pumping stations41

Figure 35. Fragility curves for tension tower 3 under different scenarios of ice loading with no wind43

Figure 36. Damaging water depth using a truncated normal for a (a) External AC unit; (b) Electrical outlet.45

Figure 37. Fragility function for electrical components with respect to amount of rainfall46

Figure 38. Fragility curves of electric components based on flood depth.....47

Figure 39. Flooding fragility curves for high voltage, medium voltage and low voltage substations and distribution centers48

Figure 40. Mean damage ratio for substations, transmission lines and power plants.....49

Figure 41. Water depth damage fragility functions for mixed utility poles.....50

Figure 42. Derived fragility functions for a water supply treatment plant.....52

Figure 43. Power grid failure probability analysis from GIC threat scenario.....53

Figure 44. Expected insulation half-life of transformers as a function of hot spot temperature.54

Figure 45. School fragility curve using Design level 2. Source: W (L) Wang, J W van de Lindt. 2022.55

Figure 46. Fragility curve of a wood-frame residential building due to atornado56

Figure 47. Total cost curves for manufacturing plant based on duration of outage57

Figure 48. Additional risk to patient due loss of electricity during a medical procedure that requires an electric medical device.58

Figure 49. Probability of unit costs due to a power outage.59

Tables

Table 1.1. Hazards for which fragility functions are included in this report.....2

Table 1.2. Fragility functions assets by identified hazard.....2

Table 2.1. The breakdown of content of the CLiP Database.....4

1.0 Introduction

Fragility curves provide the vulnerability between hazard intensity and an asset. Federal installations may include many different electricity and water infrastructure types (or assets) such as generators, wind turbines, solar PV, switch yards, substations and power lines as well as water distribution systems that could be affected by different hazards. The vulnerability of each asset is a function of its age, type of materials and maintenance. In addition, the vulnerability changes with the hazard's intensity and has a probability distribution function associated with it. For example, a hazard like a hurricane and associated flooding, earthquake, or tornado doesn't come with one probability and the value of the damage comes with its own probability function. Thus, the value of the loss is not simply the probability of the hazard times the probability of the vulnerability times the probability of the consequence as we usually do in a simple risk equation.

The solution is more appropriately approached using a *Monte Carlo* simulation to draw from appropriate distribution functions for each hazard, vulnerability and consequence for each asset. Additionally, if there are multiple assets at risk, which could affect electricity and/or water outage durations, the value at risk is a function of all the assets that lead to the outage duration, which necessarily is not one value for the hazard, vulnerability and consequence. If the analyst only uses the simple approach, the value at risk likely doesn't well represent the multivariate probability solution. Using the inappropriately defined value of risk could affect the benefit cost analysis in such a way as to choose solution that provides benefit cost ratios (BCR) greater than 1 that reduce risk but not as much as one that if properly valued could reduce the risk substantially more but didn't provide a BCR greater than 1.

Thus, the fragility functions are used in conjunction with hazard probability and consequence valuations to determine the values at risk for examination of investment grade analyses of alternative mitigation strategies. Federal analysts widely use BCR to determine if a project is cost-effective when allocating funding to projects or determining if regulatory actions or investment decisions provides more benefits than costs. For example, FEMA requires the completion of a BCR worksheet when applying for Federal disaster funds. BCR is often considered the analysis of choice because it offers an "apples-to-apples" approach to comparing projects. However, BCR analysis oftentimes requires more detailed data than simply risk equations. If an analyst was to input higher-level data, they could potentially inappropriately define the value of risk. As a result, it uses the inappropriately defined value of risk could affect the benefit cost analysis in such a way as to choose solution that provides benefit cost ratios (BCR) greater than 1 that reduce risk but not as much as one that if properly valued could reduce the risk substantially more but didn't provide a BCR greater than 1. The fragility functions in this paper can be used in conjunction with resilience valuation methodology found in "Framework for Quantitative Evaluation of Resilience Solutions: An Approach to Determine the Value of Resilience for a Particular Site" and available at https://www.pnnl.gov/main/publications/external/technical_reports/PNNL-28776.pdf

This paper seeks to make it easier for analysts who want to evaluate projects using BCR to find more publicly available data on individual asset fragility curves to fully calculate the value at risk. This paper provides a synopsis of identified resources for fragility curves for electricity and water, briefly documents their content with a summary of the hazards and assets examined and any other aspects of the resource and provides a citation and link for the resource. The paper provides examples of the fragility curves by hazard infrastructure system (electricity and water) and the associated asset type. The following hazards that affect electricity were investigated for

their fragility curves are shown in **Table 1.1**. Assets identified from the literature and databases are identified by infrastructure type and hazard in Table 1.2.

Table 1.1. Hazards for which fragility functions are included in this report

Climate Based Hazards	Non-Climate Based Hazards
Tornado Hurricane Wildfire High Wind Flood Wind and Ice Tsunami	Earthquakes Volcano Geomagnetic Storms

Table 1.2. Fragility functions assets by identified hazard

Assets	Infrastructure System	Hazards
Earthquakes		
Substation	Electricity,	Earthquakes,
Transmission and Distribution	Electricity,	Earthquakes,
Power Generation Plant	Electricity,	Earthquakes, Wind
Hydropower System	Electricity, water	Earthquakes
High Voltage Equipment	Electricity	Earthquakes
Wind Turbine	Electricity	Earthquakes
Transformer	Electricity	Earthquakes
Power Grid	Electricity	Earthquakes
Lifelines	Electricity	Earthquakes
Concrete Pole	Electricity	Earthquakes
Substations	Electricity	Earthquakes
Wind		
Wind Turbine	Electricity	Wind
Utility Pole	Electricity	Wind
Circuit Breaker	Electricity	Wind
Telecommunication Tower	Electricity	Wind
Tower Line	Electricity	Wind
Transmission line	Electricity	Wind
Transmission Tower	Electricity	Wind
Transmission Overhead Line	Electricity	Wind
Hurricane		
Transmission Tower Line	Electricity	Hurricane
Circuit Breaker	Electricity	Hurricane
Transmission Tower	Electricity	Hurricane
Solar Panel	Electricity	Hurricane
Power Grid	Electricity	Hurricane
Electrical Conductor	Electricity	Hurricane
Energy Infrastructure	Electricity	Hurricane
Residential Building		Hurricane
Nuclear Power Plant Pipping	Electricity	Hurricane
Yucca Mountain Nuclear Waste Repository	Electricity	Hurricane
Oil Pumping Station		Hurricane
Urban Gas Pipeline		Hurricane

Assets	Infrastructure System	Hazards
Electric Substation	Electricity	Hurricane
Ice Loads		
Transmission Tower	Electricity	Ice Loads
Tsunami		
Utility Pole	Electricity	Tsunami
Flood		
Building Component (AC unit / outlet)	Electricity	Flood
Electrical Component	Electricity	Flood
Power Grid	Electricity	Flood
Geomagnetic Storm		
Power Grid	Electricity	Geomagnetic Storm
Pumping Station	Water	Earthquakes
Water Treatment Plant	Water	Earthquakes
Buried Plants	Water	Earthquakes
Volcano		
Water Treatment Site	Water	Volcano
Severe Temperatures		
Distribution Transformers	Electricity	Heat (high temperature)
Loss Valuation Functions		
Manufacturing Plant	Electricity	Power outage
Health Care Equipment	Electricity	Power outage
Industrial Customers (Factories)	Electricity	Power outage
Tornado		
School Building		Tornado
Residential Building		Tornado

2.0 Earthquakes

The following section provides a synopsis of the assets and their fragility functions by asset type. Some databases like the CLiP database contain many different assets and configurations of the asset while others may report only on the fragility function of the specific asset type. Where the synopsis covers an entire database, the major components and assets will be described and a short description of how to use the database will be provided.

2.1 CLiP Lifelines Fragility Database

The CLiP Lifelines Fragility Database v 0.1.0 is a fragility function viewer developed with the financial support of a research cooperative of Oregon-based lifeline providers called Cascadia Lifelines Program (CLiP located at <https://cascadia.oregonstate.edu/>). The database was created to gather fragility functions suitable for Oregon lifelines to allow for the quality assessment of existing fragility functions and to detect missing fragility curves that may be appropriate for Oregon lifelines.¹

2.1.1 Content

Clip Lifelines Fragility Database v 0.1.0 contains fragility functions retrieved from publicly available sources such as INCORE (van de Lindt, 2019), SYNER-G (SYNER-G, 2013), HAZUS (FEMA, 2010), the Portland Bureau of Environmental Science (BES, 2018) and other published papers. The database is structured following a hierarchy of infrastructure systems, hazards, and fragility function attributes. All the fragility functions in the database except for two were developed for earthquake hazards. The other two functions are based on tornado hazards. Table 2.1 shows the breakdown of content of the CLiP Database. The table was retrieved from CLIP FRAGILITY REPORT found on the database website shown above located at <https://clip.engr.oregonstate.edu/CLiPFragilityDatabase/>.

Table 2.1. The breakdown of content of the CLiP Database

Infrastructure System	Infrastructure Subclass	Number of Fragility Functions
Electric Power System	Substation	119
	Transmission and Distribution	7
	Power Generation Plant	40
Wastewater System	Buried Pipes	70
Water System	Pumping Station	22
	Water Treatment Plant	18
	Buried Pipes	43
	Reservoir, Wells, Storage Tank	51
Transportation System	Roads	6

¹ M S Alam, B G Simpson, A R, B M J Olsen. Fragility Function Viewer. CLiP Lifelines Fragility Database v 0.1.0. School of Civil & Construction Engineering. Oregon State University. <https://clip.engr.oregonstate.edu/CLiPFragilityDatabase/>

M S Alam, B G Simpson, A R Barbosa. 2020. Defining Appropriate Fragility Functions for Oregon. A report for the Cascadia Lifeline Program. School of Civil and Construction Engineering. Oregon State University. <https://app.box.com/s/vkq345sz5rvyd49k9nnjhvu907fqnb8>

Infrastructure System	Infrastructure Subclass	Number of Fragility Functions
	Bridges	436
	Embankment	8
	Abutment	8
	Tunnel	10
	Railway Track	5
	Port and Harbor	20

2.1.2 How to use the database

The CLiP Lifelines Fragility Function viewer allows the user to exploit the database in three steps:

- **First Step:** Viewing a single fragility function using the Single Fragility Function pane. A user can choose a fragility function based on infrastructure system, infrastructure subclass, and hazard type. The user can then select the given fragility function by clicking on the check box. The Single Fragility Function pane will display the plotted fragility function and allow the user to examine it.
- **Second Step:** Comparing two or more fragility functions using the Comparison of Fragility Functions pane
After examining a single fragility function, a user may want to plot and view multiple fragility functions at once for comparison purposes. To do so, the user can search for and select several distinct functions by checking their corresponding check boxes. The Single Fragility Function pane will display the last selected fragility function; however, the Comparison of Fragility Functions pane will display all the selected functions based on intensity measures (i.e., PGA, PGV, Sa(g) ...)
- **Third Step:** Exporting fragility functions reference information using the Fragility Functions for Exporting pane

CLiP Lifelines Fragility Function viewer also allows users to download fragility functions reference information. To do so, a user should select one or multiple fragility functions and click on the EXPORT tab located in the Fragility Functions for Exporting pane. This action will create and download a csv format file containing the description of each selected function. The description includes the author and research paper that was used to develop each function. Nevertheless, the fragility functions graphs are not included in the csv file.

2.2 Concrete distribution poles

Baghmisheh and Mahsuli (2021)¹ discuss probabilistic collapse and damage models for reinforced concrete poles in electric power distribution systems and analyze the collapse and damage pattern of poles under earthquake stimulations. Structurally, the paper first develops specific element models of the H-type reinforced concrete pole and verifies these models via observed damage in previous earthquakes and anterior experimental analyses. Then, the study subjected the models to nonlinear static analyses before conducting an incremental dynamic study to evaluate the sensitivity of the seismic response and collapse mechanism of poles based on concrete strength and the direction of ground motion. Using the incremental dynamic analysis outcomes, the authors derived collapse and damage fragility models for 9 meters, 12

¹ A G Baghmisheh, M Mahsuli. 2021. "Seismic performance and fragility analysis of power distribution concrete poles". Soil Dynamics and Earthquake Engineering 150(2021)106909.
<https://doi.org/10.1016/j.soildyn.2021.106909>

meters, and 15 meters long poles by employing the maximum likelihood method. The paper notes that its proposed models give the possibility to factor in the effect of damage incurred by the power distributions lines in both the seismic study of electrified communities and seismic risk assessment of the power distribution networks.

Remarks: The intensity measures used for the fragility curves are Point Ground Acceleration (PGA) and Spectral Acceleration (Sa). Mathematical function forms are found on pages 3 and 4, and fragility function graphs are found on pages 12 and 13.

Hognestad's model for stress-strain relationship of concrete in compression is shown on Equations 1 and 2 below.

$$f_c = f'_c \left[\frac{2\varepsilon_c}{\varepsilon_o} - \left(\frac{\varepsilon_c}{\varepsilon_o} \right)^2 \right] \quad (1)$$

$$\varepsilon_o = \frac{2f'_c}{E_c} \quad (2)$$

- Where f_c = compressive concrete strength
- f'_c = maximum concrete strength
- E_c = elastic modulus
- ε_c = any strain
- ε_o = strain associated with stress f'_c

The functional forms can be seen in the three figures below (Figure 1) for 9-meter, 12-meter, and 15-meter-long poles.

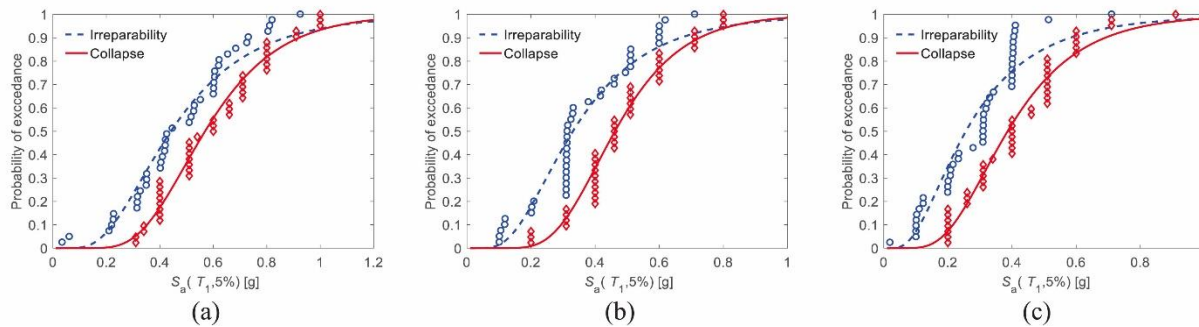


Figure 1. Fragility curves for (a) the 9 m -long, (b) 12 m-long, and (c) 15 m-long poles. Source: Baghmisheh and Mahsuli, 2021.

2.3 Transformers

Dinh et al. 2019¹ present a study about the seismic vulnerability of a hybrid mold transformer based on a dynamic approach that includes the experimental results of shaking

¹ N H Dinh, J-Y Kim, S-J Lee, K-K Choi. 2019. "Seismic Vulnerability Assessment of Hybrid Mold Transformer Based on Dynamic Analyses". 2019. Applied Sciences 9-15(2019) 3180. <https://doi.org/10.3390/app9153180>

table tests. The authors developed an analytical model whose dynamic parameters are based on the shaking table results. They used it to simulate the hybrid mold transformer before performing a reliability test to verify the analytical model. Regarding the seismic vulnerability test, the paper analyzed three critical damage states through three performance levels described in ASCE 41-17 and conducted dynamic analyses using a set of twenty earthquakes and variations of certain parameters of the mold transformers.

Remarks: The study used a 3800 kg cast resin-type hybrid mold transformer that has a maximum capacity of 1000 kVA, and its dimensions are 2110 mm (height) X 1900 mm (length) X 1030 mm (width).

The intensity measure used is Point Ground Acceleration (PGA). Mathematical fragility function forms can be found on page 10, and fragility graphs on page 19. Various graphs for critical dynamic responses effect of coil mass variation on the mold transformer are found on pages 17 and 18.

Equation 2 provides the relationship between the probability of exceedance and a specific intensity level in a log-normal distribution function. Figure 2 shows the functional form graphically.

$$P(DS|IL = x_i) = \Phi\left(\frac{\ln(x_i/\theta)}{\beta}\right) \quad (3)$$

Where: P = probability that a component response exceeds a determined performance level at a given ground motion
 DS = specified damage state
 IL = intensity level
 x_i = intensity level value
 Φ = standard normal cumulative distribution function
 θ = median of fragility function
 β = standard deviation of fragility function

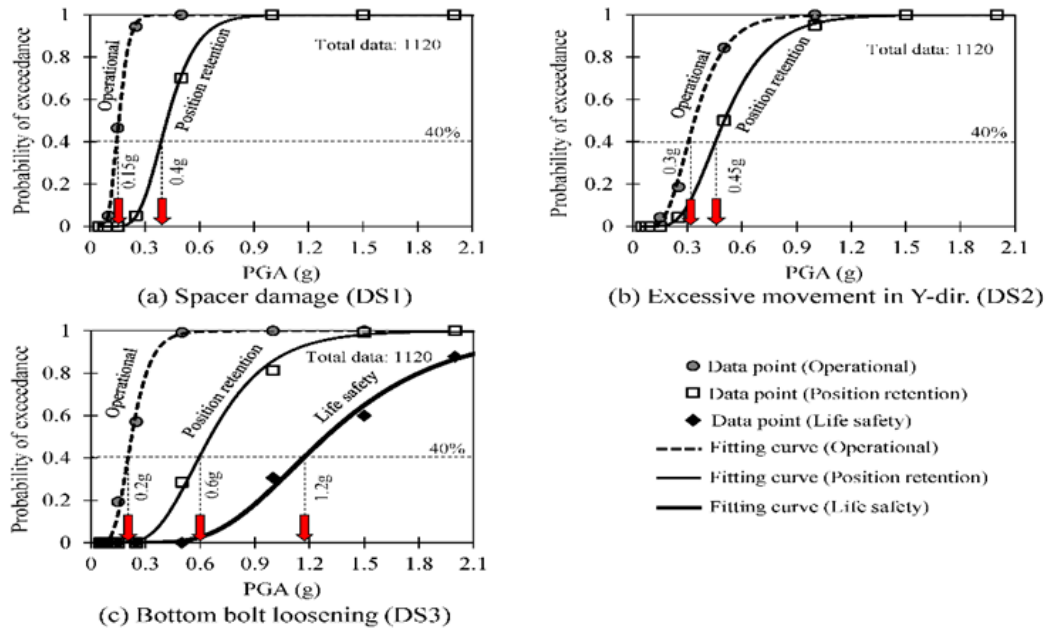


Figure 2. Fragility curves for different damage states of the mold transformer
 Source: N H Dinh, J-Y Kim, S-J Lee, K-K Choi. 2019.

2.4 Electric Substation Equipment

Mohammadpour and Hosseini(2022)¹ propose a strategy to reduce the uncertainty of electric power equipment fragility curves that are generally created using high dispersion data usually obtained by time history analyses and field investigations. The first part of their strategy consists of substituting peak ground acceleration (PGA) as intensity measure with spectral acceleration, $S_a(T_1)$, at fundamental periods of the system. The second step consists of applying $S_a(T_1) + S_a(T_2)$ as the intensity measure. The last step pertains to using a set of scenario earthquakes for time history analysis rather than randomly selected accelerograms. In the paper, the authors began by providing a succinct history of fragility curve creation for electric power equipment before presenting studies that attempted to increase the reliability of these curves. They went on to compare the results of their method with approaches from the other studies they surveyed and concluded that using $S_a(T_1)+S_a(T_2)$ leads to higher consistency.

Remarks: The electric substation equipment studied are post insulator (PI) and current transformer (CT). Multiple fragility function graphs are displayed throughout the document. However, there is not any mathematical function provided. The following graph can be found on page 16.

¹ S Mohammadpour, M Hosseini. 2022. “Dispersion reduction of the analyses data for more reliable fragility curves of selected electric substations equipment”. Bulletin of Earthquake Engineering 20 (2022) 5519-5544. <https://link.springer.com/article/10.1007/s10518-022-01391-2>

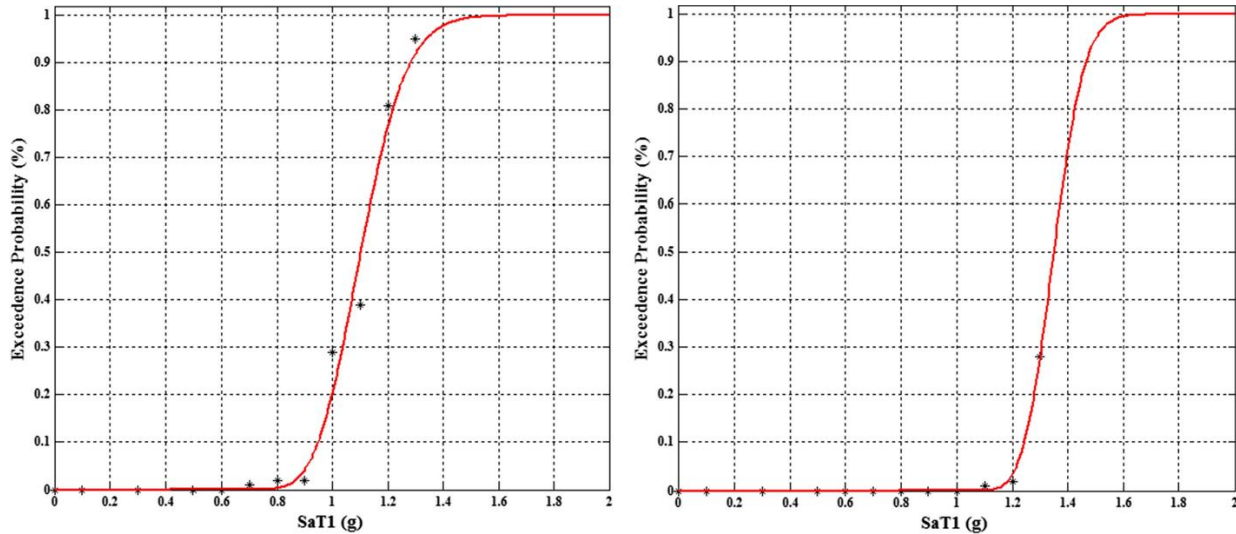


Figure 3. Exceedance probability of 63KV post insulator, DI values of 11.72 MPa(left) and 23.44 MPa (right).

Source: S Mohammadpour, M Hosseini.2022

2.5 High-Voltage Electrical Equipment

Liu et al. (2020)¹ use the cumulative Gaussian distribution function to analyze the relationship between the damage rate of high-voltage equipment and the instrumental seismic intensity. The study is based on the damage data of high voltage equipment in the Wenchuan earthquake in China in 2008. The paper employs the Kriging interpolation method to calculate the instrumental seismic intensity at 110kv and above voltage level and estimates the instrumental seismic intensity at strong motion monitoring stations before using the Gaussian function to develop the fragility curves of six types of high-voltage equipment. The equipment types include circuit breaker, transformer, current mutual inductor, voltage mutual inductor, lighting arrester, and isolating switch. In conclusion, Liu et al. (2020) indicate that transformers are the most vulnerable type of equipment to earthquake hazards, followed by lightning arresters.

Remarks: The intensity measure used is instrumental seismic intensity. The explanation for its calculation is given in section 2 of the paper. Several mathematical functions are provided on pages 2,3,4 and 6, while fragility function graphs are found on page 8.

Equation 4 and 5 represents the cumulative Gaussian distribution function that shows the relationship between instrumental seismic intensity and the damage rate of high voltage equipment. Figure 2.4 shows the functional form graphically.

$$F(x) = 0.5 + 0.5erf\left(\frac{x - \mu}{\sigma\sqrt{2}}\right) \quad (4)$$

¹ R Liu, M Xiong, D Tian.2020. "Relationship between Damage Rate of High-Voltage Electrical Equipment and Instrumental Seismic Intensity". Advances in Civil Engineering (2021). Article ID 5104214, 10 pages. <https://doi.org/10.1155/2021/5104214>

Where: $F(x)$ = distribution function
 x = random variable following Gaussian distribution
 σ = standard deviation
 μ = expected value

$$\text{erf}(x) = \frac{2}{\sqrt{\pi}} \int_0^x e^{-t^2} dt \quad (5)$$

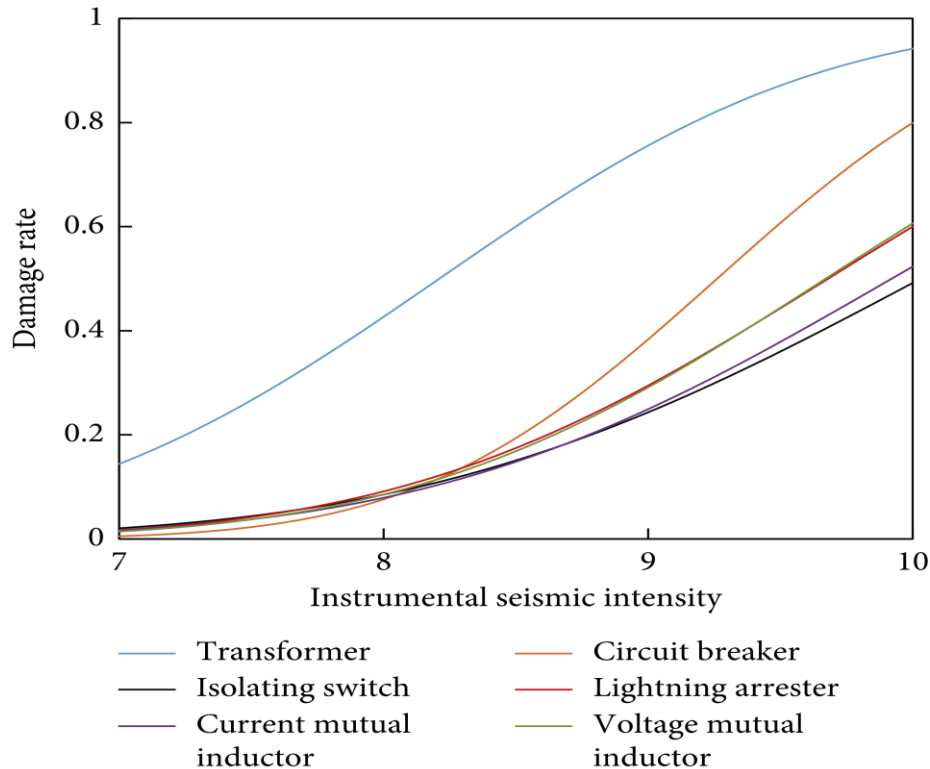


Figure 4. Damage probability curves for all kinds of high voltage electrical equipment.
 Source: R Liu, M Xiong, D Tian. 2020

2.6 Electric Power Stations

Cavalieri et al.¹ wrote the sixth chapter of a book series entitled Geotechnical, Geological and Earthquake Engineering (GGEE, volume 27) which covers various fragility curves topics and related assets such as waste-water systems, oil, and gas networks, electric power stations, and more. In their work, Cavalieri et al. propose a survey of fragility models for the parts of electric power networks by first presenting the major features of an electric power network and its relevant taxonomy. Then, the authors highlighted the key details for a few chosen papers on fragility functions before selecting specific fragility curves most relevant for use in the European context. The selection is based on the data used for the models and the adopted simulation methodology.

¹ F Cavalieri, P Franchin, P E Pinto. 2014. "Fragility Functions of Electric Power Stations". In: Pitilakis, K., Crowley, H., Kaynia, A. (eds) SYNER-G: Typology Definition and Fragility Functions for Physical Elements at Seismic Risk. Geotechnical, Geological and Earthquake Engineering, vol 27. Springer, Dordrecht. https://doi.org/10.1007/978-94-007-7872-6_6

Remarks: Point ground acceleration (PGA) is the intensity measure used for all fragility graphs except one. Also, all the curves are in lognormal cumulative distribution functions expressed in the logarithmic standard deviation beta (β) and the logarithmic mean lambda (λ).

Equations 6 and 7 on page 11 of the chapter define lambda and beta, while the graphs that display fragility curves are found on pages 16 to 13; and 25 to 26. Figure 2.5 shows the fragility curves for small generation plants.

$$\lambda = \ln(m) \quad (6)$$

$$\beta = 0.74 * [\ln(75^{th} \text{ percentile}) - \ln(25^{th} \text{ percentile})] = 0.74 * IQR \quad (7)$$

Where λ = logarithmic mean

m= median

β = logarithmic standard deviation

0.74= value from range 0 to 0.75 in the selected intensity measure

IQR= interquartile range of the associated normal distribution

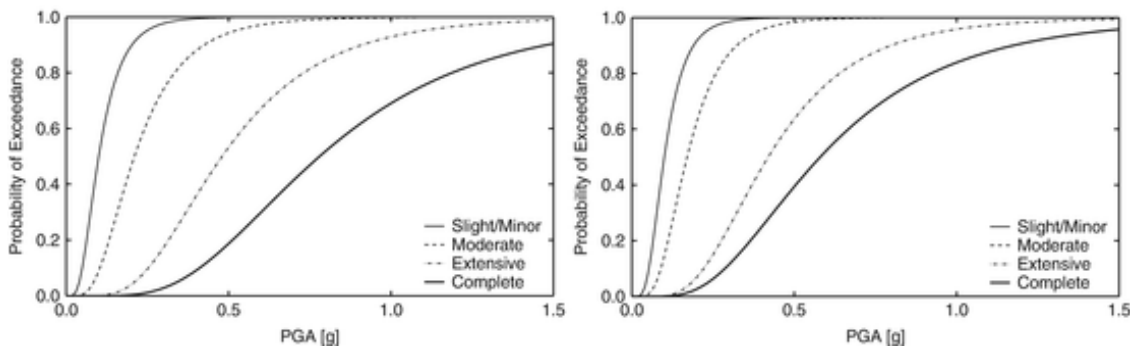


Figure 5. Fragility curves for small generation plants, with anchored (left) and unanchored (right components).

Source: F Cavalieri, P Franchin, P E Pinto. 2014.

2.7 Hydropower Systems

Lin and Adams (2007)¹ present the results of their study on the vulnerability of the components of Canadian hydropower installations under earthquake excitations. Their analysis focused on eastern and western Canadian dams and their associated components, such as switchyards, hydropower plants, complementary equipment, and transmission towers. To carry out the study, the authors calculated the seismic vulnerability for designated hydropower components and calculated the seismic hazard using the model built by the Geological Survey of Canada. According to the paper, the switchyards and power plants are the most fragile parts of a hydropower system.

Remarks: The intensity measure used is point ground acceleration (PGA). Figure 2.6 is found in page 8 of the article and graphically shows the damage probabilities of the hydropower system.

¹ L Lin, J Adams. 2007. "Lesson for the Fragility of Canadian Hydropower Components under Seismic Loading". https://www.earthquakescanada.nrcan.gc.ca/hazard-alea/2007/9CCEE/9CCEE_Lin_Adams_p1186.pdf

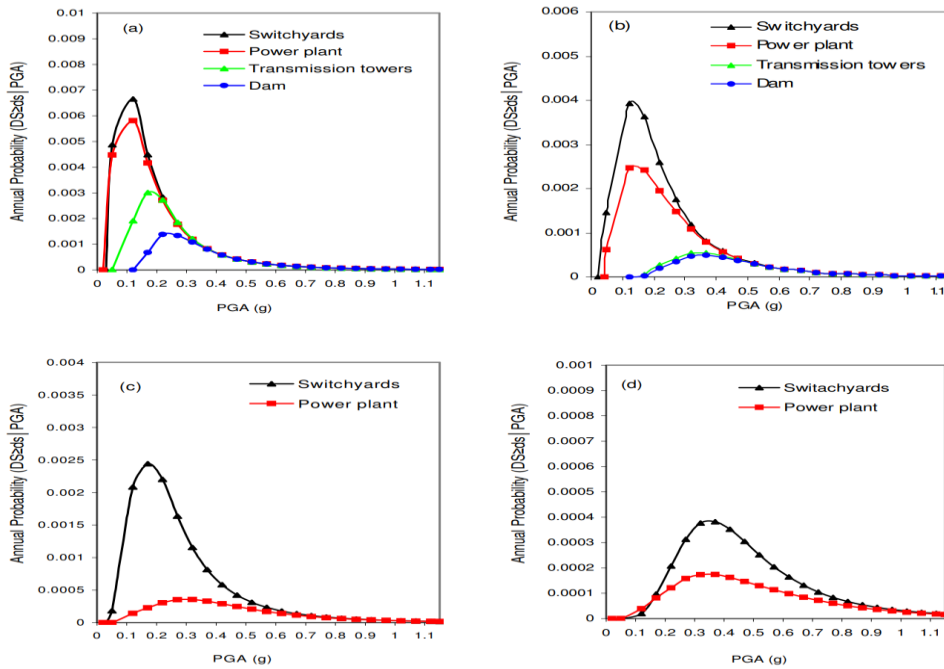


Figure 6. Probability distributions for hydroelectric components at the selected site. (a) Slight damage, (b) light damage, (c) Moderate damage, (d) Heavy damage.
 Source: Lin, Adams. 2007

2.8 Power Grid

Veeramany et al. (2018)¹ promote the risk modeling framework for high-impact, low-frequency power grid events developed by the Pacific Northwest National Laboratory. The paper illustrates the framework application for seismic and geomagnetic hazards and presents the method used to conduct fragility evaluation, hazard analysis, post-event restoration, and consequence assessment.

Remarks: The intensity measure used is PGA. The demonstration of the framework application is based on transformers, buses, and transmission towers. Figure 2.7 shows the resulting fragility curve for transformers. It is found on page 2 of the article. The mathematical functions given in the study pertain to geomagnetism.

¹ A Veeramany, G A Coles, S D Unwin, T B Nguyen, J E Dagle. 2018. "Trial Implementation of a Multihazard Risk Assessment Framework for High-Impact Low-Frequency Power Grid Events". IEEE systems journal, 12-4 (2018).
<https://ieeexplore.ieee.org/stamp/stamp.jsp?tp=&arnumber=8016567>

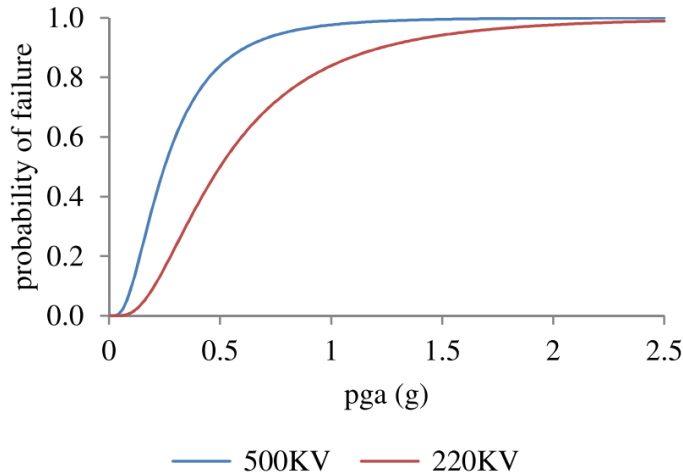


Figure 7. Cumulative distribution function (capacity curves) for the transformer. Source: A Veeramany, G A Coles, S D Unwin, T B Nguyen, J E Dagle. 2018.

2.9 Wind Turbine

Mohammad-Amin (2015)¹ presents a document comprising three papers covering the wind energy production industry. The third paper is where he discusses wind turbine fragility curves in the context of seismic and wind excitations. In this paper, Mohammad-Amin (2015) uses a novel finite element model to evaluate the nonlinear dynamic behavior of a 5-MW NREL wind turbine submitted to various earthquakes and wind forces. The author verified the validity of the model by employing static and modal pushover analysis. Then, he used intensity measures and engineering demand parameters obtained from nonlinear incremental dynamic analysis to study the probability the exceeding multiple damage states.

Remarks: The intensity measures used are spectral acceleration (Sa), and wind speed expressed in meter per second (m/s). The equation below provides a lognormal distribution function representing the relationship between various intensity measures and the probability of exceeding a given damage state. This equation can be found on page 114 of the primary document.

$$F_{DS}(IM) = \Phi \left[\frac{\ln \left(\frac{IM}{\mu_{IM}} \right)}{\sigma_{IM}} \right] \quad (8)$$

Where: IM = intensity measure of earthquake (PGD, Sa, PGA, Sd)

μ_{IM} and σ_{IM} = respectively mean and log standard deviation of the intensity measure

$\Phi(\cdot)$ = cumulative distribution function of standard normal variable

DS = damage level assigned to a certain engineering parameter or damage measure

¹ A Mohammad-Amin.2015. "Dynamic behavior of operational wind turbines considering aerodynamic and seismic load interaction." Doctoral Dissertations. Paper 2375. https://www.researchgate.net/publication/280025120_Dynamic_behavior_of_operational_wind_turbines_considering_aerodynamic_and_seismic_load_interaction

The figure below, found on page 116 of the primary document, graphically illustrates the fragility curve of the 5-MW NREL wind turbine

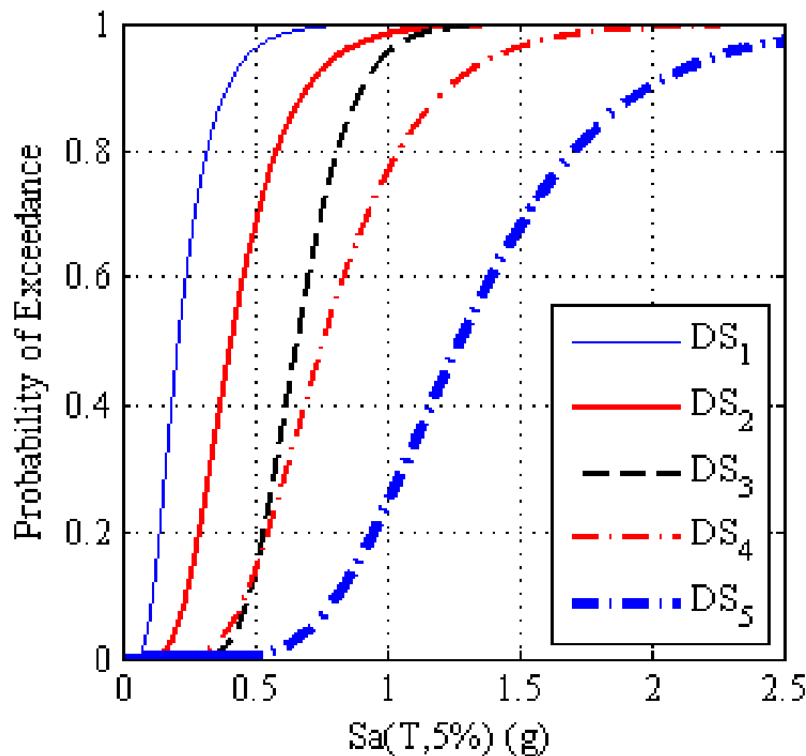


Figure 8. Fragility Curve for different damage states of the 5-MW NREL wind turbine for 2.5 m/s wind speed.

Source: A Mohammad-Amin. 2015

2.10 Lifelines

Argyroudis and Pitilakis (2014)¹ consider that lifelines consist of utility systems (including electric power distribution) and transportation networks that provide vital services to contemporary societies. Their work focuses on explaining the various efforts deployed by the research community to understand the seismic vulnerability of the various components of the lifelines. For that reason, this paper provides an explanation for the seismic vulnerability evaluation of lifelines and introduces both an inventory and taxonomy of the potentially vulnerable elements of these networks. Moreover, the authors explain the foundation of earthquake hazard analysis before indicating that fragility curves are the most common tools for seismic risk assessment. Besides, Argyroudis and Pitilakis (2014) discussed the various aspects of the fragility models, including the types of models, performances, and uncertainties, reliabilities.

¹ S A Argyroudis, K Pitilakis. 2014. "Seismic Vulnerability Assessment: Lifelines". Encyclopedia of Earthquake Engineering. Chapter: Seismic Vulnerability Assessment:Lifelines. http://dx.doi.org/10.1007/978-3-642-36197-5_255-1

Remarks: This paper discusses the work done to understand the seismic vulnerability of lifelines and the steps taken to conduct the analysis. It presents examples of fragility curves from pages 19 to 22, among which the following one.

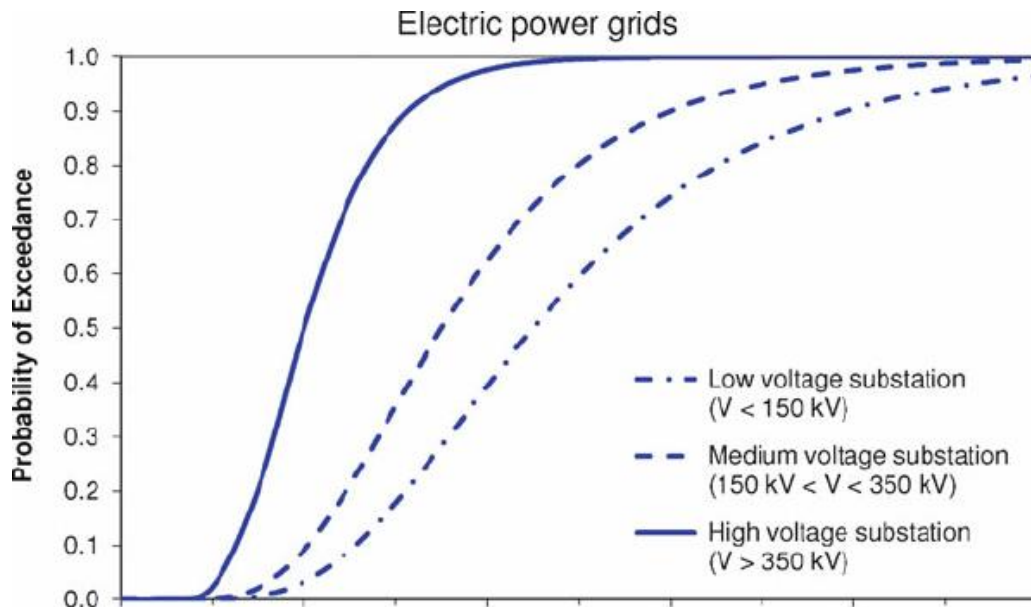


Figure 9. Empirical fragility curves for power grids made up of substations of different voltages based on data from US west coast earthquakes.

Source: S A Argyroudis, K Pitilakis. 2014.

3.0 Wind

3.1 Wind Turbine

Del Campo et al. (2020)¹ present a study performed on 1 MW, 2.5 MW, and 3.5 MW land-based wind turbines under earthquake-induced hazards. In the study, the three wind turbines are in parked condition, are similar to the ones installed in Mexican wind farms in terms of dimensions and are located in a fictional place determined based on Mexico's wind capacity distribution. To conduct the analysis, the authors collected ground motions records from real events that happened close to the assumed wind farm site and developed Tuned Mass Dampers (TMDs) models for each of the three turbines. The paper estimated the parameters for the TMDs models by conducting harmonic analyses, whereas the optimal parameters were evaluated from time history responses obtained.

Remarks: The intensity measure used is Point Ground Acceleration (PGA). Mathematical fragility function forms and graphs are found in section 5 of the paper entitled "Development of Fragility Curves".

Equation 9 provides a linear equation representing the median of the response in an earthquake case. Source: J Osvaldo Martin del Campo, A. Pozos-Estrada, O Pozos-Estrada. 2020.

$$\widehat{DP}(IM) = (a_1\mu + a_2\xi + a_3\varphi + a_4)IM \quad (9)$$

Where :

\widehat{DP} = median of structural response

μ = mass ratio of tuned mass damper

ξ = damping ratio of tuned mass damper

φ = Frequency ration of tuned mass damper

IM = represents the PGA of the ground motion as a fraction of g

a_1 to a_4 = model coefficients

¹ J Osvaldo Martin del Campo, A Pozos-Estrada, O Pozos-Estrada. 2020. "Development of fragility curves of land-based wind turbines with tuned mass dampers under cyclone and seismic loading." Wind Energy 24-7(2020) 737-753. <https://doi.org/10.1002/we.2600>

The fragility curves for the three different sizes of wind turbines are shown in Figure 10.

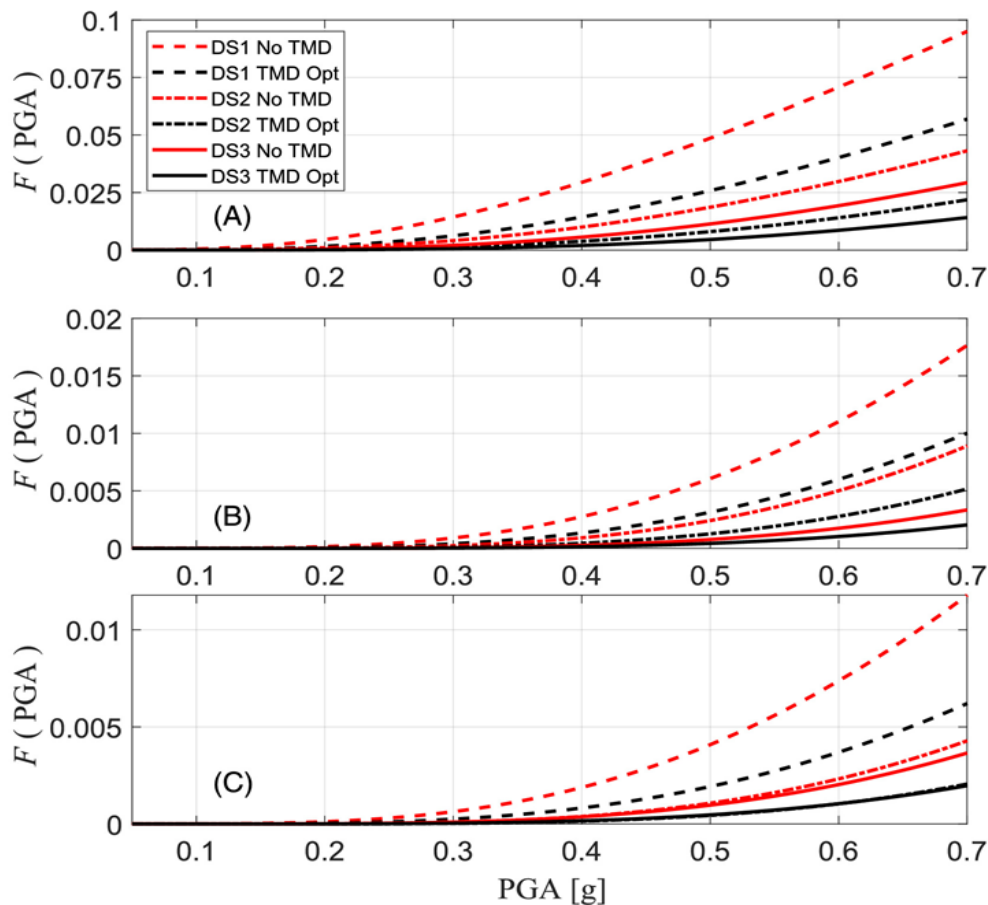


Figure 10. Fragility curves different size wind turbines: (A) 1 MW wind turbine, (B) 2.5 MW wind turbine, (C) 3.3 MW wind turbine.

Source: J Osvaldo Martin del Campo, A Pozos-Estrada, O Pozos-Estrada. 2020.

3.2 Wind Turbine

Zuo et al. (2020)¹ begin their work by developing an elaborate three-dimensional finite element model of the NREL 5 MW wind turbine in ABAQUS. Secondly, they explicitly modeled the wind turbine towers and blades to realistically evaluate the aerodynamic loads and structural behaviors of the turbine. In the study, the authors accounted for the material, stiffness, and damping uncertainties to produce the probabilistic demand models for the turbine tower and blades subjected to aerodynamic and sea wave loading. Zuo et al. tested these models in a probabilistic frame before developing the fragility curves for both the blades and tower under operating and parked conditions. In the paper, the considered damage states (DS) for the tower and blades are based on the ultimate limit states and serviceability.

¹ H Zuo, K Bi, H Hao, Y Xin, J Li, C Li. 2020. "Fragility analyses of offshore wind turbines subjected to aerodynamic and sea wave loadings." *Renewable Energy* 160 (2020) pp. 1269-1282. <https://doi.org/10.1016/j.renene.2020.07.066>

Remarks: The intensity measure used is wind speed expressed in meters per second (m/s). Mathematical functions are listed on pages 4 to 8, and fragility function graphs are on pages 10 and 12.

The following equation provides a power law functional expression of the structural demands for wind turbines under combined wind and sea wave stimulations.

$$D_w = m(v_w)^n \text{ or } \ln(D_w) = lmm + n\ln(v_w) \quad (10)$$

Where: D_w = median wind-induced out-of-plane displacement of the wind turbine
 v_w = mean wind speed at the hub height
 m and n = coefficients obtained from regression estimation

The fragility graphs for the blades under parked condition are shown in the figure below.

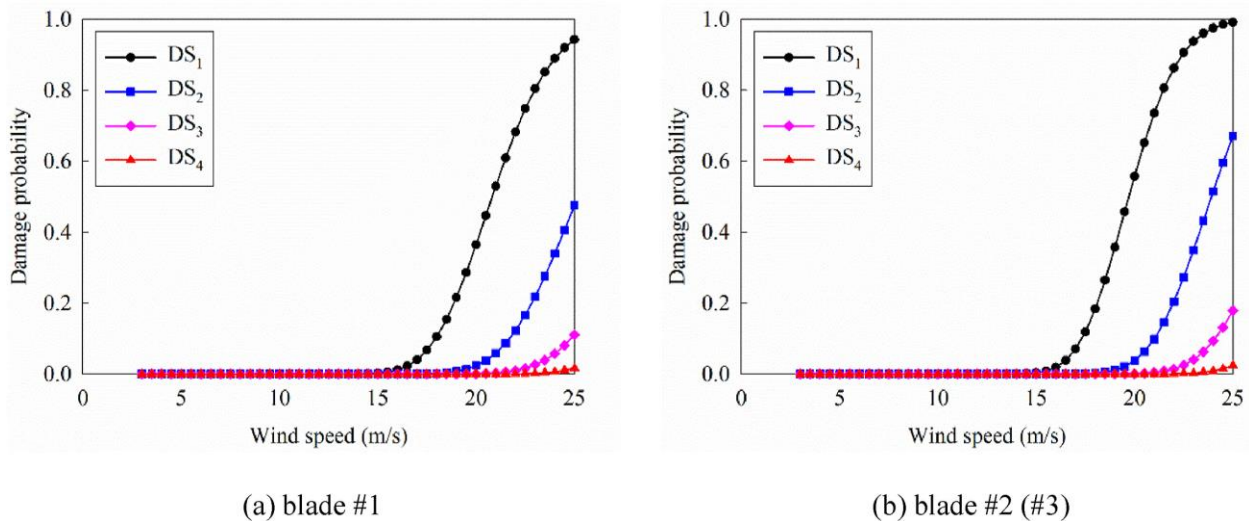


Figure 11. Fragility curves for wind turbine blades in parked conditions.
 Source: H Zuo, K Bi, H Hao, Y Xin, J Li, C Li. 2020.

3.3 Utility Poles

Salman (2014)¹ discusses a method for performing fragility analysis of steel and timber utility poles under hurricane wind hazards. He used a Monte Carlo simulation to produce the fragility curves by accounting for wind loads, uncertainty in strength, and geometry. Then, Salman conducted a life-cycle analysis by comparing the timber and steel poles before concluding that steel poles were more advantageous than timber poles in terms of life-cycle cost and reliability.

Remarks: The intensity of measure used is miles per hour (mph). On pages 48 and 50, we find mathematical expressions of the fragility curves, whereas pages 52 to 56 contain figures that graphically display the fragility functions.

¹ A M Salman 2014. "Age-dependent fragility and life-cycle cost analysis of wood and steel power distribution poles subjected to hurricanes". Master's Thesis, Michigan Technology University.2014 <https://digitalcommons.mtu.edu/cgi/viewcontent.cgi?article=1779&context=etds>

Equation (11) estimates the fragility models of the steel and timber poles. The figure below graphically presents the fragility curve of new timber and steel poles.

$$F_R(V) = \phi \left[\frac{\ln \left(\frac{v}{m_R} \right)}{\xi_R} \right] \quad (11)$$

Where: $F_R(v)$ = structural fragility
 m_R = median strength
 v = wind speed
 ξ_R = logarithmic standard deviation of capacity

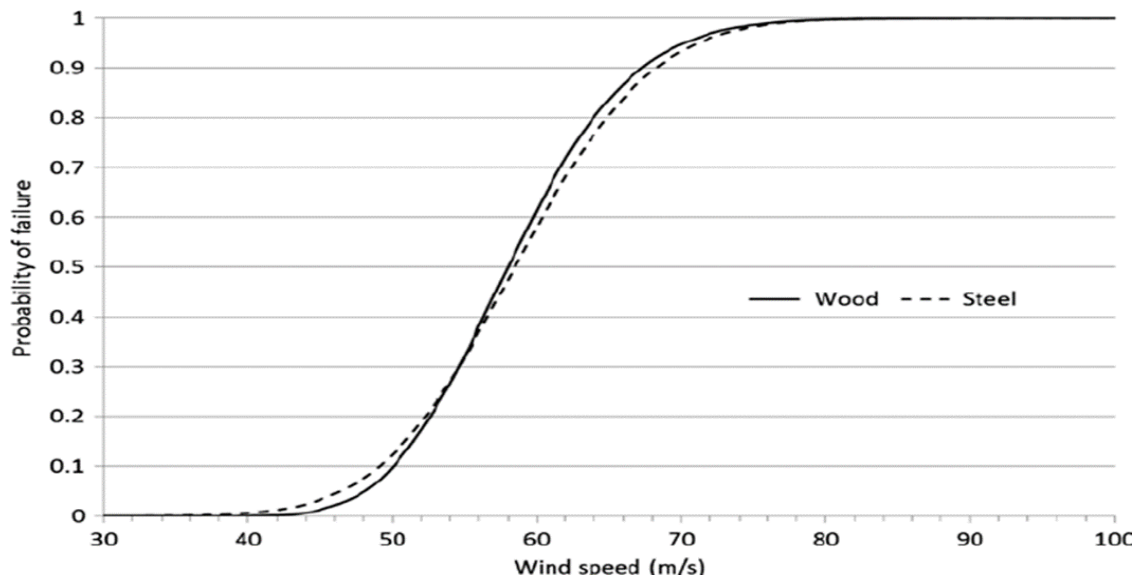


Figure 12. Fragility curves of new wood and steel poles.

Source: A M Salman.2014

3.4 Utility pole

Kim et al. (2021)¹ introduce a novel data-driven framework to support the decision-making process for utility maintenance in extreme weather events. After collecting imagery data from Google Street Views to analyze the geometric characteristics of utility poles, the authors examined the probability of failure of the poles using a three-dimensional artificial city model. To test the practicality of the model, Kim et al. (2021) applied their model to a Texan case study. They concluded that the proposed approach is capable of using public visual data to evaluate the fragility of utility pole networks.

Remarks: The intensity measure used is wind speed expressed in meters per second (m/s).

The figure below shows the fragility curves of a leaning utility pole

¹ J Kim, M Kamari, S Lee, Y Ham.2021. "Large-Scale Visual-Data-Driven Probabilistic Risk Assessment of Utility Poles Regarding the Vulnerability of Power Distribution Infrastructure Systems." Journal of Construction Engineering and Management. <https://ascelibrary.org/doi/10.1061/%28ASCE%29CO.1943-7862.0002153>

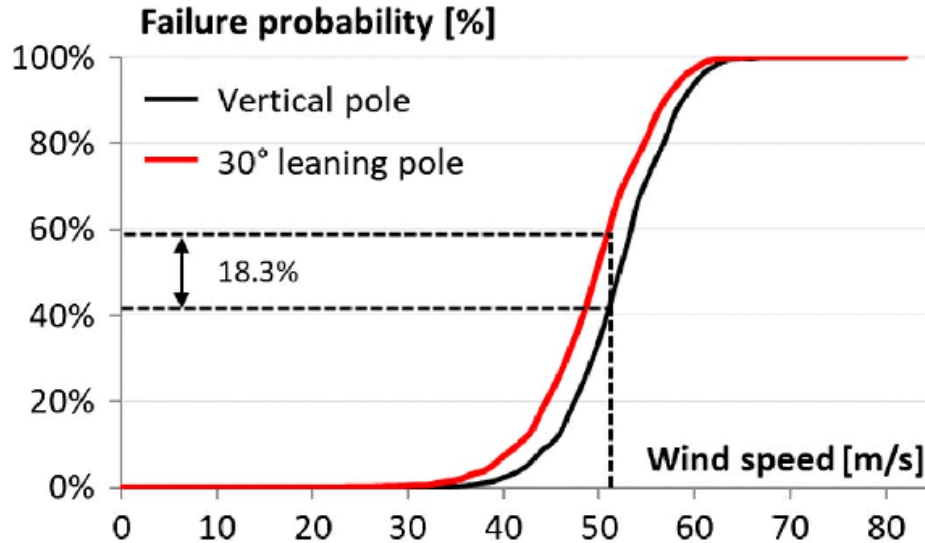


Figure 13. Wind fragility curves pole and 30 degree leaning pole showing that leaning can increase failure probability. Source: J Kim, M Kamari, S Lee, Y Ham. 2021.

3.5 Utility Pole

Allen-Dummas et al. (2019)¹ document the existing analytical resources for sensitivity evaluation of electric grid components under hazardous weather conditions. Moreover, they highlight the insufficiencies in the research on quantitative methods available for studying electric grid components' fragility. The third section of the report explains how to quantify component damage or break down, and sections 5 and 6 detail the different vulnerability sources to electric transmission and generation systems. To learn more about essential functions for sensitivity analysis, one must read section 4 of the report.

Remarks: The paper presents only one fragility curve figure to graphically illustrate commonly used fragility functions. The intensity measure used in the graphs is wind speed expressed in meters per second (m/s).

¹ M R Allen-Dumas, B KC, C I Cunliff. 2019. "Extreme Weather and Climate Vulnerabilities of the Electric Grid: A Summary of Environmental Sensitivity Quantification Methods." ORNL/TM-2019-1252. <https://www.energy.gov/sites/prod/files/2019/09/f67/Oak%20Ridge%20National%20Laboratory%20EIS%20Response.pdf>

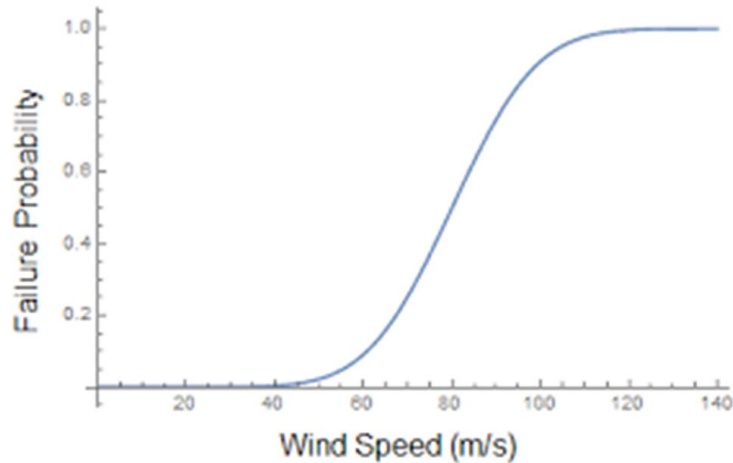


Figure 14. Example fragility curve for wind damage to utility poles. Source: M R Allen-Dumas, B KC, C I Cunliff. 2019.

3.6 Circuit Breaker

Shahzad (2022)¹ suggests a transient stability risk evaluation methodology that integrates circuit breaker failure and severe weather. In the context of the paper, severe weather refers to windstorms. After associating all random variables such as fault type, load demand, faulty location, and faulty clearing time by using probability density functions, Shahzad (2022) conducted a Monte Carlo simulation to sample these probability density functions. The study was carried out under three conditions. These conditions are for the normal condition (base case), a condition including circuit breaker failures, and severe weather condition. The paper notes that an IEEE 14-bus and IEEE 39-bus tests were performed to validate the proposed method. Based on the paper, the results of the tests reveal that severe weather and circuit breaker failures must be considered in the transient stability risk estimation process.

Remarks: Intensity measure is wind speed expressed in meters per second (m/s). Pages 4 and 5 contain mathematical functions, whereas pages 8 and 9 present visual representations of IEEE-14 bus test system and IEEE-39 bus test system. On page 6, we find equation 12 and the following figure, which represents the mathematical and graphical relationship between transmission line failure probability and wind speed.

$$Pl(w) = \begin{cases} Pl^n, & \text{if } w < w_{critical} \\ Pl(w), & \text{if } w_{critical} \leq w < w_{collapse} \\ 1, & \text{if } w \geq w_{collapse} \end{cases} \quad (12)$$

Where: $Pl(w)$ = failure probability of any transmission line as a function of wind speed
 w = wind speed
 Pl^n = failure probability under normal weather conditions. It is assumed to be 0.01
 $w_{critical}$ = wind speed after which failure probability significantly increases
 $w_{collapse}$ = the failure probability of lines is 1

¹ U Shahzad (2022). "Transient stability risk assessment framework incorporating circuit breaker failure and severe weather." Australian Journal of Electrical and Electronics Engineering <https://doi.org/10.1080/1448837X.2021.2023072>

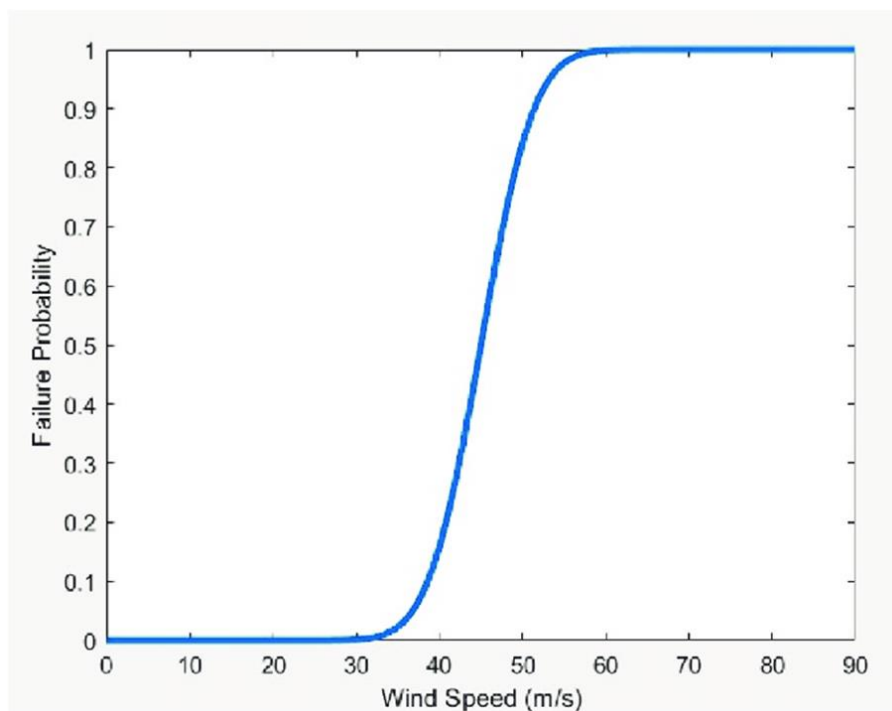


Figure 15. Fragility curve for transmission lines.
Source: U Shahzad. 2022.

3.7 Telecommunication Towers

Bilionis and Vamvatsikos (2019)¹ focused on developing fragility functions for standard Greek telecommunication towers under several combinations of wind and icing conditions that can occur during the lifetime of the towers. After conducting non-linear dynamic assessments to evaluate the fragility of the towers to wind and or icing loads, Bilionis and Vamvatsikos (2019) simulated wind loads using a 3D wind field that accounts for the temporal and spatial variation of wind speed over the entire surface of the tower. To analyze the impact of ice on the telecommunication towers, the authors examined a set of distinct uniformly thick layers of ice that augment the structure's weight. The outcomes of this paper suggest that wind has a major impact on the telecommunication, tower especially when coupled with ice accumulation.

Remarks: The intensity measure used for wind hazards is wind speed expressed in meters per second (m/s). Three ice layer thicknesses are considered. They are 15 mm, 30 mm, and 45 mm. The typical tower studied in the paper supports dish antennas, is 48 meters tall, and is designed after European specifications for locations lower than 10 km from the coastline.

A few mathematical functions are found on pages 5,6,8, and 11. The following equation represents a lognormal cumulative function of the fragility curve considered in the paper.

¹ D V Bilionis, D Vamvatsikos. 2019. "Wind performance assessment of telecommunication towers: A case study in Greece." *Eccomas Proceedia COMPDYN* (2019) 5741-5755. DOI: <https://oa.mg/work/10.7712/120119.7342.19629>

$$P(C|IM = x) = \Phi\left(\frac{\ln\left(\frac{x}{\theta}\right)}{\beta}\right) \quad (13)$$

Where $P(C|IM=x)$ = probability that a value of Intensity Measure equal to x will cause the tower to fail.

$\Phi()$ = standard normal cumulative distribution function

Θ = median of the fragility function

β = standard deviation

$\ln IM$ = dispersion of IM

The figure below graphically presents fragility curves for different wind and ice thickness combinations.

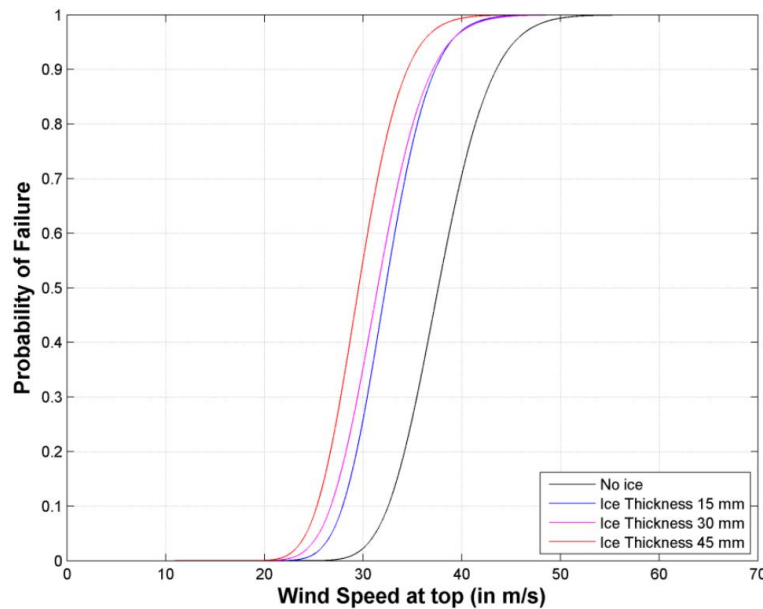


Figure 16. Fragility curves for wind speed and ice thickness combinations.

Source: D V Bilonis, D Vamvatsikos.2019.

3.8 Tower lines

Huang et al. (2018)¹ recommend a dynamic resilience constrained economic dispatch (RCED) method to improve operational resilience during severe weather events. The study uses local weather forecast data to part the entire electrical network into severe weather impacted zone and normal state zone. The paper notes that two penalty terms are introduced to the suggested RCED objective function to prevent the power system from turning into a self-organized critical system.

Remarks:

The equation below represents the transmission fragility function used in the paper.

¹ L Huang, X Cun, Y Wang, C S Lai, L L Lai, J Tang, B Zhong.2018. "Resilience-Constrained Economic Dispatch for Blackout Prevention." IFAC-PapersOnLine 51-28(2018) 450455.
<https://doi.org/10.1016/j.ifacol.2018.11.744>

$$p_w = \begin{cases} 0, & \text{if } w < w_{critical} \\ p_{hw}, & \text{if } w_{critical} \leq w \leq w_{collapse} \\ 1 & \text{if } w \geq w_{collapse} \end{cases} \quad ()$$

Where w = wind speed

$w_{critical}$ = wind speed at which transmission line’s failure probability begins,

$w_{collapse}$ = wind speed at which the transmission line will be nearly broken (30m/s, 60m/s)

The fragility graph used in the paper is based on (Panteli et al. 2017), and it shows the fragility curves for a transmission tower and a transmission tower line. The intensity measure used is the wind speed in meters per second, m/s.

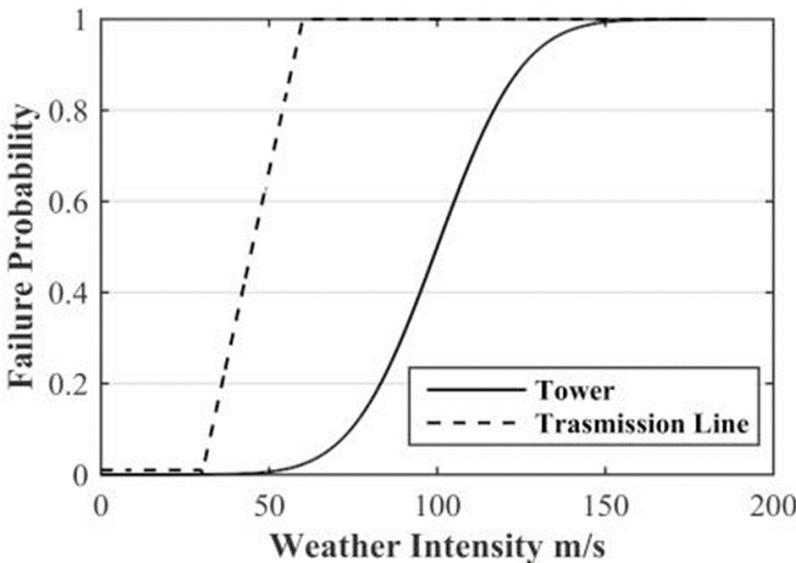


Figure 17. Wind-related fragility curves of transmission lines and towers.
 Source: L Huang, X Cun, Y Wang, C S Lai, L L Lai, J Tang, B Zhong. 2018.

3.9 Transmission lines

Fu et al. (2019)¹ developed a fragility analysis approach which integrates wind loads and the uncertainties of structural elements into a numerical model. The presented model applies to transmission line that are under wind excitations. Fu et al. (2019) analysis begins with a basic model with two lines and one tower that is used to enhance calculation accuracy. Then, they validated the model using a full tower-line system in dynamic and static positions. To conduct the fragility analysis, the authors built uncertainty models, and performed a regression analysis after completing a nonlinear dynamic assessment.

Remarks: The graph below is fragility function displayed in the paper. The intensity measure used is wind speed expressed in meters per second (m/s).

¹ X Fu, H Li, L Tian, J Wang.2019. “Fragility Analysis of Transmission Line Subjected to Wind Loading.” Journal of Performance of Constructed Facilities 33-4(2019).
<https://ascelibrary.org/doi/10.1061/%28ASCE%29CF.1943-5509.0001311>

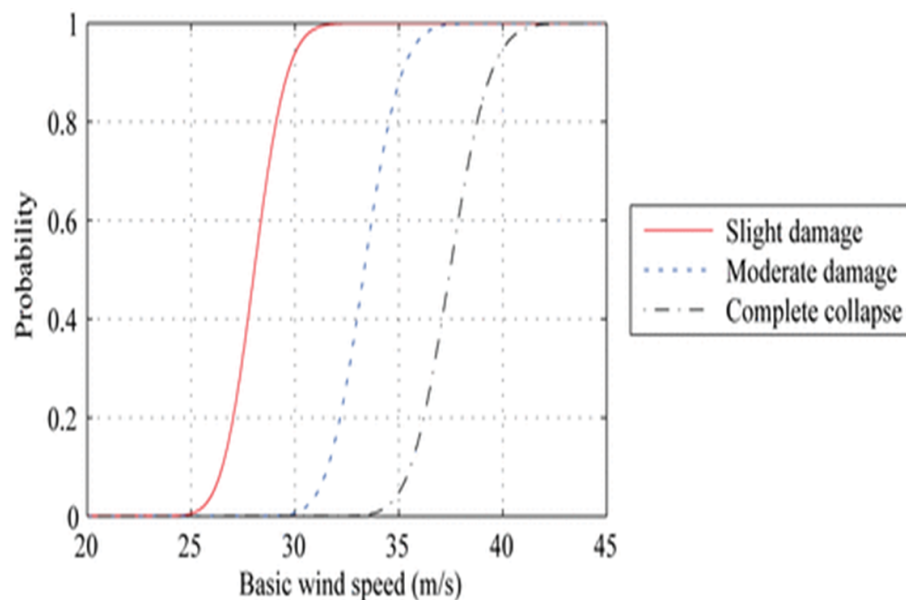


Figure 18. Fragility of transmission lines based on wind speed
Source: Fu et al. (2019)

3.10 Communication Tower

Tian et al. (2020)¹ investigate a communication tower's collapse process and fragility under wind hazards. The first step of this investigation began with creating a finite-element (FE) model of a 60-meter-tall tower that fell due to wind pressure. The authors used ABAQUS (version 6.10) to create the finite-element model and examined the wind-induced reaction mechanism using the Tian-Ma-Qu material model. On the other hand, they relied on a dynamic explicit approach to simulate tower collapse with various wind charge angles using the incremental dynamic analysis framework. According to the study, the Tia-Ma-Qu material model allows to simulate communication tower collapse effectively.

Remarks: The intensity measure used is wind speed expressed in meters per second.

The figure below represents a tower fragility functions under different wind charge angles.

¹ L Tian, X Zhang, X Fu. "Collapse simulations of communication tower subjected to wind loads using dynamic explicit method." 2020. Journal of Performance of Constructed Facilities 34-3(2020). <https://ascelibrary.org/doi/abs/10.1061/%28ASCE%29CF.1943-5509.0001434>

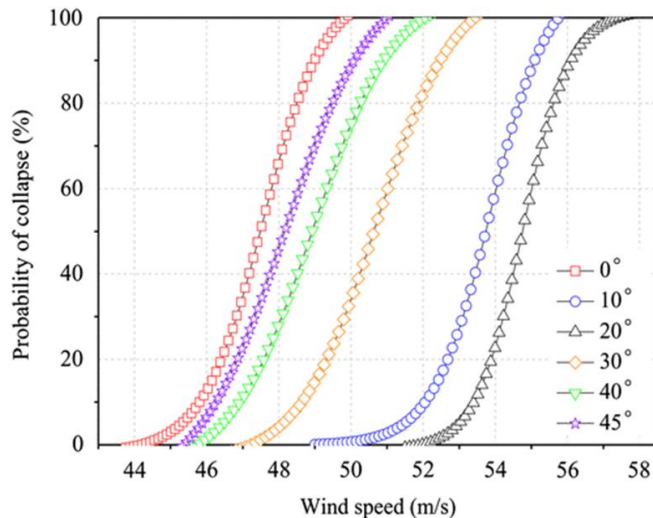


Figure 19. Communication tower fragility due to wind speed
Source: Tian et al. (2020)

3.11 Transmission Towers

Wang et al. (2022)¹ examine how downbursts impact transmission towers by studying five towers of different sizes under moving or static downburst wind influences. They compared the behavior of the towers under downburst wind and normal wind. They concluded that the reaction of transmission towers under downburst depends on the distance between the towers and the center of the downburst. Sections 2 and 3 of the paper explain the numerical models used in the study, whereas sections 4.1, 4.2, and 4.3 examine the response of the transmission towers under specific situations.

Remarks: The intensity measure used is wind speed. Multiple mathematical models are laid out in the paper on pages 3 to 5. The following one express wind speed at any given time in the wind field:

$$U(z, t) = \bar{U}(z, t) + \tilde{U}(z, t) \quad (14)$$

The graph below shows wind speed of downburst and normal wind in different angles.

¹ Z Wang, F Yang, Y Wang, Z Fang. 2022. "Study on wind loads of different height transmission towers under downbursts with different parameters." *Journals Buildings* 12-2(2022) 193.
<https://doi.org/10.3390/buildings12020193>

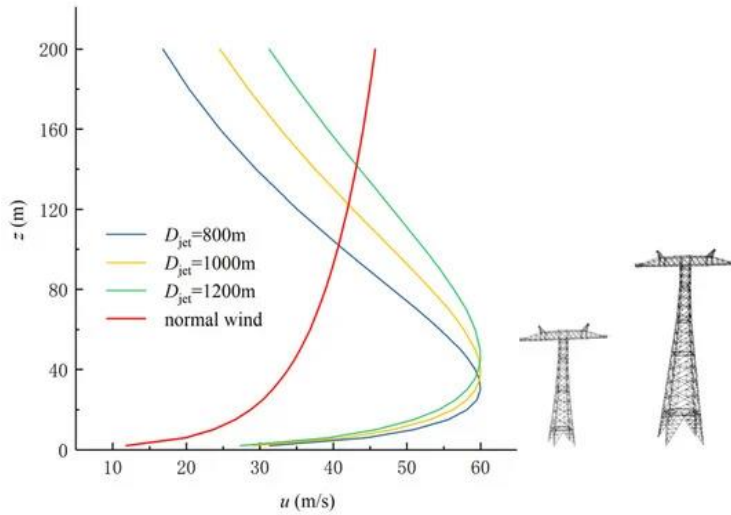


Figure 20. Profiles of normal wind and downburst with different jet diameters. Source: Z Wang, F Yang, Y Wang, Z Fang. 2022.

3.12 Transmission Overhead Line

Jamieson et al. (2020)¹ demonstrate a method that permits the visualization of the relationship between overhead line failure rates and wind hazards in case of severe wind conditions. The paper argues that the recommended method facilitates the determination of vulnerable areas of overhead line networks and the quantification of the wind impact. The study, uses line failure models, network, and reanalysis data to develop spatially resolved line failure probability while considering asset exposure and altitude. The authors claim that their method can help in resilience planning that relies on forecasted weather data and that it also constitutes a robust method of portraying weather-related failure rates of overhead lines.

Remarks: The intensity measure used is wind speed expressed in meters per second, m/s. The equation below represents the probability of failure of any line:

$$p(\text{fault}) = 1 - e^{-\lambda\delta t} \quad (15)$$

- Where p (fault) = fault probability within a given time-step
- λ = failure rate
- δt = assumed to be 1 and failure rate is in per-hour terms

The figure below shows the overhead line fragility curve showed in the study.

¹ M R Jamieson, G Strbac, K R W Bell. 2020. "Quantification and visualisation of extreme wind effects on transmission network outage probability and wind generation output." IET Smart Grid 3-2(2020) 112-122. <https://doi.org/10.1049/iet-stg.2019.0145>

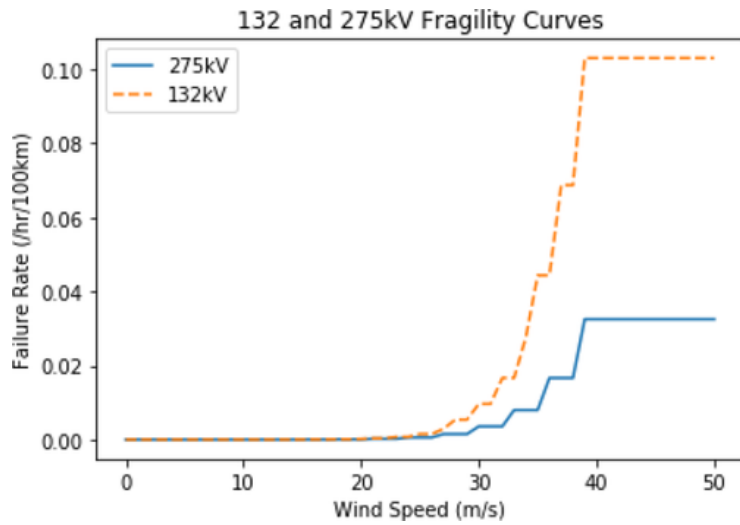


Figure 21. OHL fragility curve used in the proposed study.
 Source: M R Jamieson, G Strbac, K R W Bell. 2020.

4.0 Hurricane

4.1 Transmission Tower Line

Xue et al. (2020)¹ examine the consequences of hurricane-induced transmission tower failure and damage on the performance of the power transmission network. They developed a fragility model for a transmission tower line and improved the computational effectiveness of the fragility analysis by carefully choosing their sample size and utilizing wind speed convention. The article also evaluates the performance of the fragility models by investigating the productivity of a synthetic transmission system during Hurricane Harvey.

Remarks: The intensity measure used is meters per second (m/s). The paper displays various mathematical functions on pages 3 to 7 and fragility function graphs on page 6.

Equation 16 expresses the relationship between a transmission tower line's failure and damage probability under a given wind speed. The figure below shows that relationship graphically.

$$F_R(V) = P[l > LS | \bar{v}_{10} = V] \quad (16)$$

Where $F_R(V)$ = damage and failure probability

LS = limit state

l = simulated response compared with the limit state

\bar{v}_{10} = mean speed at 10 m

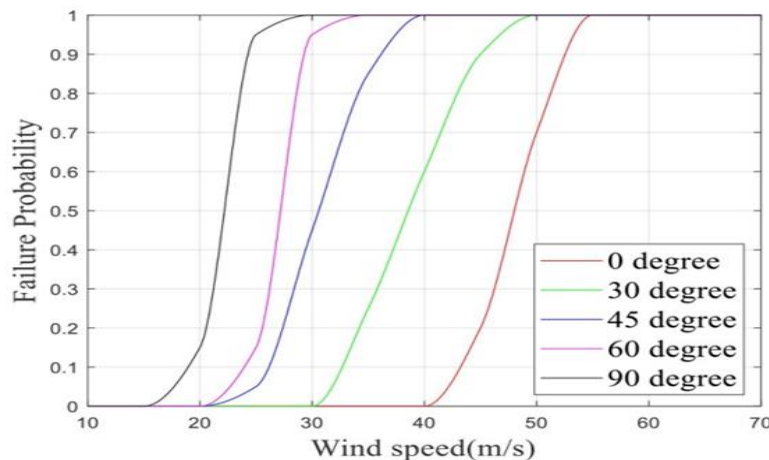


Figure 22. Fragility Curve Tower-line System based different wind angles and wind speed.

Source: J Xue, H Mohammadi, X Li, M, Sahraei-Ardakani, G Ou, Z Pu. 2020.

¹ J Xue, F Mohammadi, X Li, M Sahraei-Ardakani, G Ou, Z Pu. 2020. "Impact of transmission tower-line interaction to the bulk power system during hurricane." Reliability Engineering and System Safety 203 (2020) 107079. <https://doi.org/10.1016/j.res.2020.107079>

4.2 Transmission Towers

Ma et al. (2021)¹ study proposes a component-based fragility model that is meant to capture the realistic performance of transmission towers subjected to hurricane stimulations. The paper also develops a fragility curve assessment structure that balances efficiency and accuracy. According to the authors, the prevalent procedures used for fragility curve estimation for transmission towers are based on dynamic or static analyses, which overlook relevant details of tower connections, such as rational stiffness. Therefore, they introduced an innovative model that uses a modal superposition method and a spectral representation technique to directly simulate the load transferred from the cables to the towers. Also, Ma et al. (2021) developed a complex finite model including tower joints information and validated their method using a series of tests.

Remarks: The intensity measure is the maximum sustained wind speed (V_{ms}) expressed in m/s. In the paper, the proposed model is applied to two transmission towers that differ by size of their parts.

There are multiple mathematical functions listed in the paper on pages 4, 5, and 8. Fragility graphs are found on pages 16,17 and 18

Equation 17 is part of a series of equations used to determine the capacity of electric tower structural members. The figure shows a graphical representation of the fragility function of a tower.

$$F_a = \left[1 - \frac{1}{2} \left(\frac{KL/r}{C_c} \right)^2 \right] F_y ; \quad \frac{KL}{r} \leq C_c \quad (17)$$

Where F_a = tower member capacity

F_y = yield stress

L = unbraced length

r = radius of gyration

K = effective length coefficient

C_c = column slenderness ratio separating inelastic and elastic buckling

¹ L Ma, M Khazaali, P Bocchini. 2021. "Component-based fragility analysis of transmission towers subjected to hurricane wind load." *Engineering Structures* 242 (2021) 112586.
<https://doi.org/10.1016/j.engstruct.2021.112586>

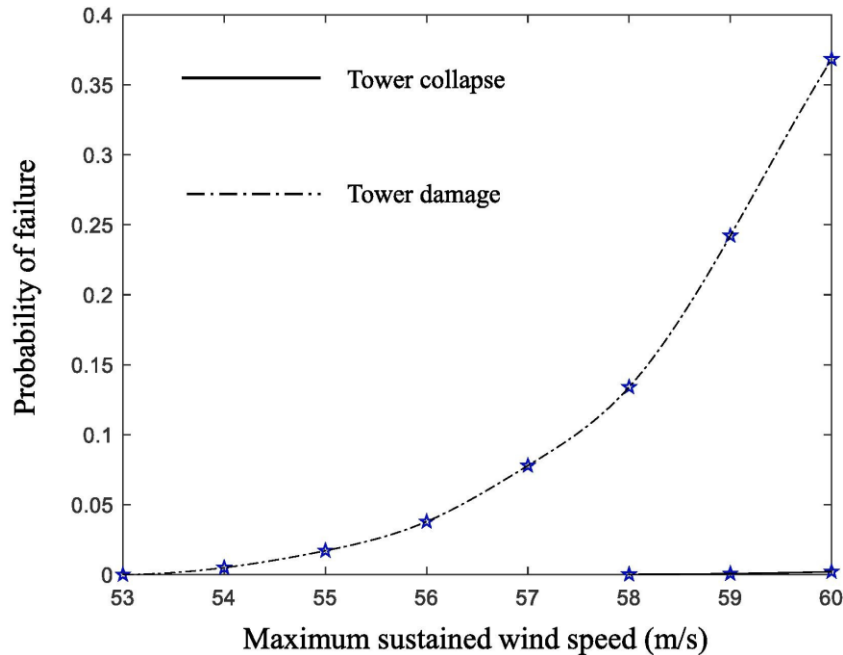


Figure 23. Fragility curves for transmission towers under 90° wind direction
Source: L Ma, M Khazaali, P Bocchini. 2021.

4.2.2 Transmission Tower

Sang et al. (2020)¹ propose an integrated framework that includes weather forecast information in preventive power system operation. According to the article, the model's objective is to help reduce power outages during hurricanes. The proposed method begins with developing a finite-element structural model of a transmission tower. Then, weather data is used as input to determine the transmission lines' probability of failure, which is added within a day-ahead unit commitment model. Simulation studies were carried out on the IEEE 118-bus system subjected to synthesized Harvey and Irma hurricanes to validate the model.

Remarks: The intensity measure used is wind speed expressed in meters per second (m/s). The paper highlights that further investigation is necessary to ameliorate the proposed model's computational efficiency and its application to large-scale real-world systems.

Mathematical functions are found on pages 5, 6, and 7, and a fragility graph is found on page 6. Equation 18 shows that under structural wind fragility, the association between failure probability and damage at any given wind speed V is expressed as follows:

$$F_R(V) = P[l > LS/V_{10} = V] \quad (18)$$

Where $F_R(V)$ = damage and failure probability

V = wind speed

LS = limit state

¹ Y. Sang, J. Xue, M. Sahraei-Ardakani and G. Ou, "An Integrated Preventive Operation Framework for Power Systems During Hurricanes," in IEEE Systems Journal, vol. 14, no. 3, pp. 3245-3255, Sept. 2020, doi:10.1109/JSYST.2019.2947672. <https://ieeexplore.ieee.org/document/8889714>

The figure below graphically portrays the fragility function.

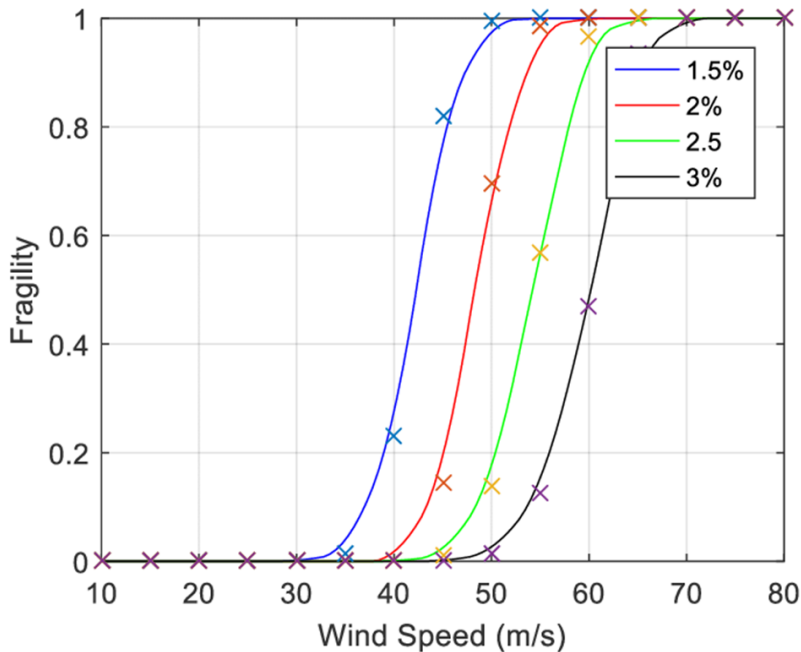


Figure 24. Wind fragility curve of a transmission tower.

Source: Y. Sang, J. Xue, M. Sahraei-Ardakani and G. Ou. 2020.

4.3 Solar Panel

Ceferino et al. (2021)¹ describe an integrative model whose function is to estimate solar generation during hurricanes. Their methodology is based on a stochastic approach that combines solar irradiance quantification, a model for irradiance decay during hurricanes, a tropical cyclone hazard model, and solar panel vulnerability. Based on the paper, the presented stochastic model can be incorporated into resilience models for larger grids and has a broad range of applicability.

As far as the fragility function of solar panels, the authors developed a function with a lognormal shape based on standard solar panel design parameters. They also observed that the fragility function was developed for rooftop solar panels but can be applied to ground-mounted panels. Besides, the paper signals that the fragility functions present certain uncertainties that come from the randomness in the relationship between wind speed and the panel components.

Remarks: The intensity measure used is wind speed expressed in 3-second gust speed. The following equation is the mathematical expression of the lognormal fragility function used in the paper. It represents the probability of panel failure and is found on page 16.

$$p = \Phi\left(\frac{\ln(w) - \ln(\bar{w})}{\beta}\right) \quad (19)$$

¹ L Ceferino, N Lin, D Xi. 2021. "Stochastic Modeling of Solar Generation During Hurricanes." PREPRINT (Version 1) available at Research Square <https://doi.org/10.21203/rs.3.rs-797974/v1>

Where p = panel's structural failure
 $\Phi(.)$ = standard normal cumulative distribution function
 W = wind that the solar panel experiences
 \bar{w} and β = equal 58 ms^{-1} (3-second maximum wind) and 0.3 respectively

The following figure graphically displays the above mathematical function.

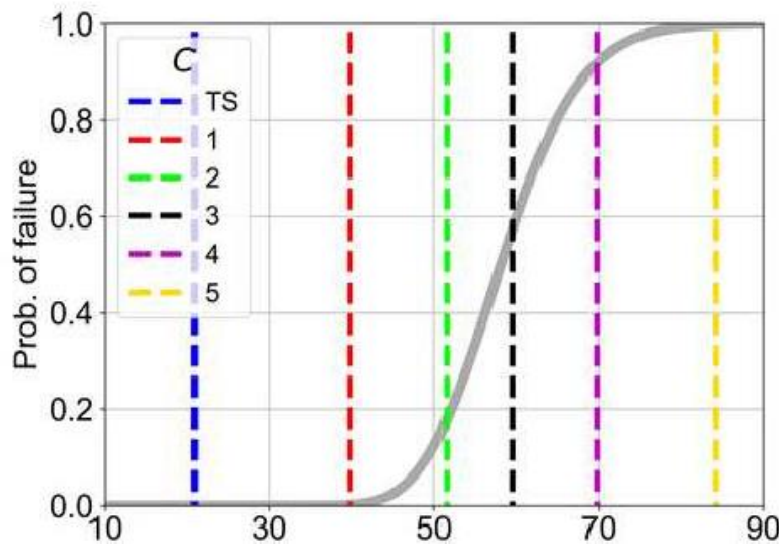


Figure 25. Fragility function for solar panels due to wind speed
 Source: L Ceferino, N Lin, D Xi. 2021.

4.4 Power Grid

Watson and Etemadi (2020)¹ examine hurricane exposure, propose a model for power stations and another model for damage to the electrical transmission grid parts. They use techniques including restoration cost and a Monte Carlo simulation to forecast resilience factors such as damage to power generation systems. In the study, Watson and Etemadi (2020) modeled the electrical grid of the Energy Reliability Council of Texas based on synthetic grid data and performed a case study based on hurricane Harvey.

Remarks: The intensity measure is 3-second gust wind speed expressed in miles per hour (mph). A fragility curve function for each component of the power grid was selected from the literature and can be found on pages 4 and 5.

The equation below represents the selected fragility curve for substations. This function is based on HAZUS-MH 4 internal damage tables for various damage levels as a function of the peak wind speed and terrain type.

$$P(D \geq d_j | w_i) = \Phi \left(\frac{\ln w_i - \mu_{j,k}}{\sigma_{j,k}} \right) \quad (20)$$

¹ E B Watson, A H Etemadi. 2020. "Modeling Electrical Grid Resilience Under Hurricane Wind Conditions With Increased Solar and Wind Power Generation." IEEE Transactions on Power Systems 35-2(2020) pp. 929-937. <https://doi.org/10.1109/TPWRS.2019.2942279>

Where $\Phi(.)$ = normal cumulative distribution function
 $\mu_{j,k}$ and $\sigma_{j,k}$ = logarithmic mean and standard deviation of the j^{th} damage state and terrain type k .
 μ and σ = parameters for substation fragility curves.

The graph below shows fragility curves for the various plants.

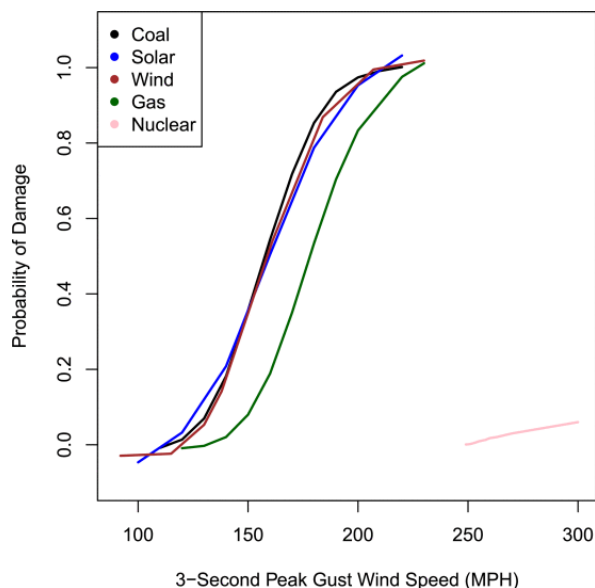


Figure 26. Fragility curves for different types of power plants.
 Source: E B Watson, A H Etemadi. 2020.

4. 5 Electrical Conductors

Ma et al. (2020)¹ present a probabilistic framework for developing fragility models of electrical transmission conductors subject to hurricane hazards. While the proposed framework accounts for uncertainties in the conductor capacity and wind hazard, a modal superposition technique was used to model the mechanical behavior of the conductors before a finite element analysis was carried out to validate the model. To obtain the capacity of the conductor, the authors employed a *Monte Carlo* simulation and used the first-order reliability method to calculate the conductors' damage and failure probabilities. According to Ma et al. (2020) their method offers a significant computational advantage because it allows for the development of a fragility curve in about 10 seconds with a high level of accuracy.

Remarks: The intensity measures used in the paper are maximum sustained wind speed expressed in meters per second (m/s) and wind direction or angle of yaw defined in degree.

In the article, various mathematical functions can be found on pages 3 to 10, and fragility functions can be found on pages 11 to 13.

¹ L Ma, P Bocchini, V Christou. 2020. "Fragility models of electrical conductors in power transmission networks subjected to hurricanes." *Structural Safety* 82 (2020) 101890.
<https://doi.org/10.1016/j.strusafe.2019.101890>

The equation below represents the probability of failure of a three phases transmission line:

$$P_{line} = 1 - \prod_{i=1}^n (1 - P_i)^3 \quad (21)$$

Where: P_i = probability of failure of the i^{th} conductor
 n = the number of spans in the transmission line

The following figure represents fragility curves for conductor with different length.

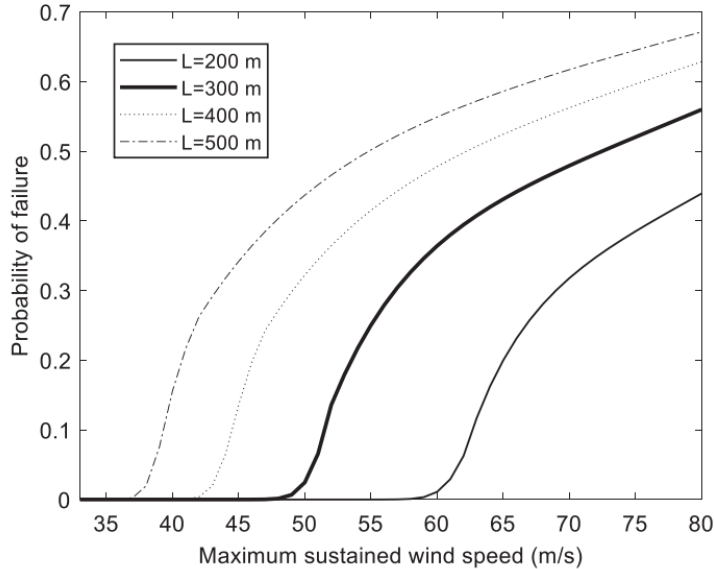


Figure 27. Fragility curves for conductor based on wind speed with span length of 200,300,400, and 500 meters.

Source: L Ma, P Bocchini, V Christou. 2020.

4.6 Energy Infrastructure

Bennett et al. (2021) propose an energy system optimization framework that accounts for hurricane risks by combining infrastructure fragility functions and hurricane probability. The model evaluates the possibility of altering grid architecture, and the possibility to modify the fuel mix and grid hardening strategies while incorporating hurricane effects and climate mitigation measures. The authors applied the model to the case of Hurricane Maria, which hit Puerto Rico in 2017, and used Tools for Energy Model Optimization and Analysis (Temoa) to evaluate the grid design and operation over a given period.

Remarks: The paper does not include a mathematical model for creating a fragility curve. However, it shows an equation that can be used to calculate the remaining operable infrastructure capacity after a hurricane ravage.

$$X_{t,n} = X_{t,n-1} \times (1 - p_f(W_s)) \quad (22)$$

Where $X_{t,n}$ = operable capacity of technology t during the nth model year,
 $X_{t,n-1}$ = operable existing capacity of technology t during the previous model year

p_f = probability of failure from the fragility curve
 W_s = peak hurricane speed of the nth model year

The figure shows the correlation between wind intensity and failure of various elements of the power system.

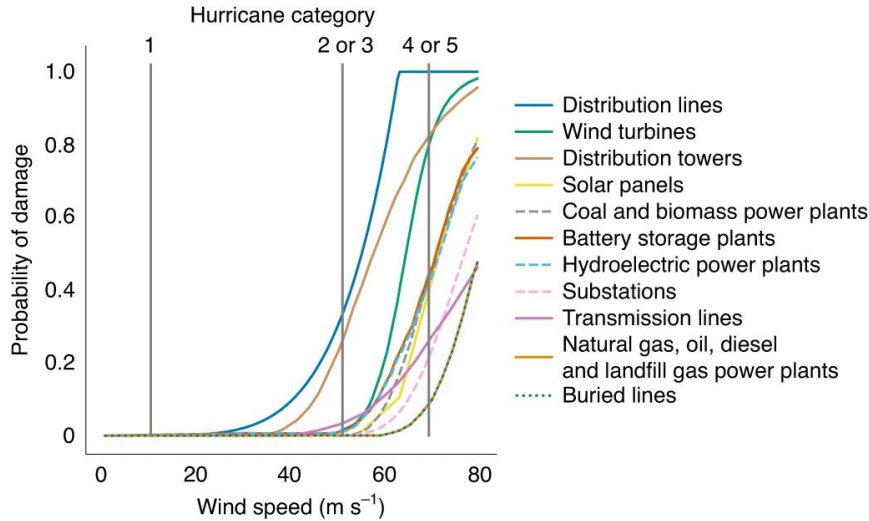


Figure 28. Fragility curves by technology based on wind speed
 Source: J A Bennett, C N Trevisan, J F DeCarolis et al. 2021.

4.7 Residential Buildings

Yue, 2012¹ illustrates in his document a risk-cost-benefit approach for estimating destruction risks and the cost-effectiveness of alleviation methods for residential infrastructures adopting scenario-case and life-cycle analysis. The presented approach combines a probability model of the occurrence and severity of natural hazards, a structural system fragility approach to indicate the conditional probability of destruction, and a model of anticipated expenses during different services. Yue argues that his framework can help improve design and construction standards and contribute to community response planning to face disasters. Besides, the article mentions that several parameters that are difficult to estimate yet import in risk evaluation are discussed for their importance in hazard alleviation decision-making.

Remarks: The intensity measure used is wind speed expressed in miles per hour, mph.

The figure below represents a fragility curve displayed in the paper.

¹ Y Li. 2012. "Assessment of damage risks to residential buildings and cost-benefit of mitigation strategies considering hurricane and earthquake hazards. Journal of Performance of Constructed Facilities 26-1(2012). <https://ascelibrary.org/doi/10.1061/%28ASCE%29CF.1943-5509.0000204>

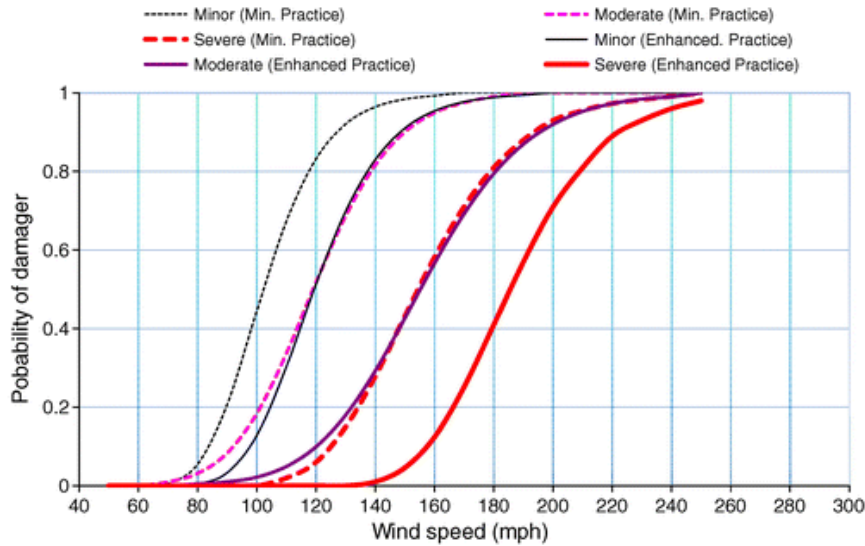


Figure 29. Fragility function for residential buildings based on wind speed
 Source: Y Li. 2012

4.8 Nuclear Power Plant Piping

Kim et al. (2019)¹ propose a quantitative failure benchmark for piping systems, which is necessary for the seismic fragility assessment of nuclear power installations against hazardous situations. The study employed the in-plane cyclic loading test to recommend a quantitative failure benchmark for steel pipe elbows in nuclear power plants. Then, the authors conducted a nonlinear analysis through a finite element framework and compared the outcomes with test results to validate the efficiency of the employed finite element model. Moreover, the study determined the collapse load point from the analysis and carried out a seismic fragility evaluation for the piping system of the Brookhaven National Laboratory and Nuclear Regulatory Commission standard model.

Remarks: The intensity measure used is point ground acceleration. The equation below shows the probability of damage of the structure under seismic excitation.

$$P_f(a) = \int_0^\infty P_R(a, x_R) \left[\int_0^{x_R} P_c(x) dx \right] dx_R \quad (23)$$

- Where a = arbitrary seismic load
- P_R = probability density function
- P_c = probability density function of the capacity

The following graph shows a fragility curve developed by using the collapse load point as a failure specification.

¹ S-W Kim, B-G Jeon, D-G Hahm, M-K Kim. 2019. "Seismic fragility evaluation of the base-isolated nuclear power plant piping system using the failure criterion based on stress-strain". Nuclear Engineering and Technology 51-2(2019) 561-572. <https://doi.org/10.1016/j.net.2018.10.006>

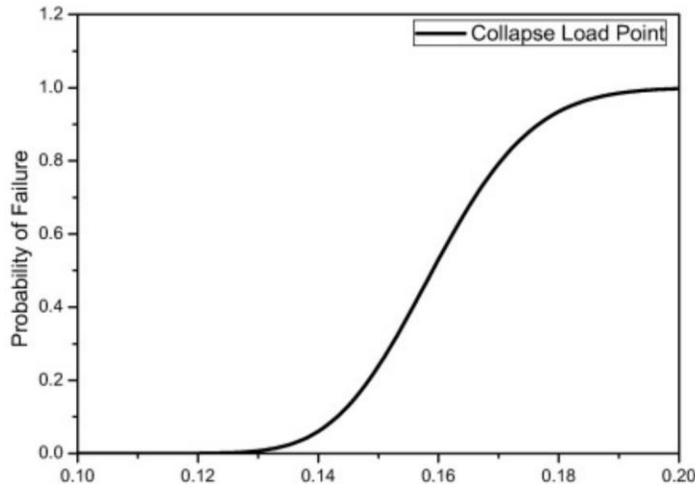


Figure 30. Seismic fragility curve for nuclear plant piping using the collapse load point as a failure criterion

Source: S-W Kim, B-G Jeon, D-G Hahm, M-K Kim. 2019.

4.9 Yucca Mountain Nuclear Waste Repository

Biswajit Dasgupta’s (2017)¹ report focuses on the Yucca Mountain site. The U.S Department of Energy determined seismic events as valid natural threats at the Yucca Mountain site during pre-closure and post-closure time frames and wants to take all safety measures to avoid catastrophes. In that vision, Dasgupta’s report documents the data recorded and examined to contribute to the preparatory activities supporting the evaluation of the DOE pre-closure safety study. Dasgupta mentions that the study’s objective is to quantify the probability of failure for structures, systems, and components (SSCs) important to safety (ITS) and to estimate the rate of occurrence of events. The paper remarks that the U.S. Nuclear Regulatory Commission provided Interim Staff Guidance (ISG), in which the seismic vulnerability of equipment is expressed as the conditional probability of failure for a specified level of seismic intensity. The seismic intensity considered are spectral ground acceleration and peak ground acceleration. Hazard and fragility curves are integrated through numerical integration or closed form solution. It must be noted that part of this paper’s goal is to detail the methodologies used to quantify the fragility parameters that affect the performance of SSCs ITS.

Remarks: The seismic probability of failure of an SSC ITS is given by the equation below.

$$P_F = - \int_0^\infty P_{f/a} \left(\frac{dH(a)}{da} \right) da \quad (24)$$

Where P_F = seismic performance of an SSC ITS
 $H(a)$ = annual probability of exceedance of ground motion level
 $P_{f/a}$ = fragility curve of the structure

¹ B Dasgupta.2017. “Evaluation of Methods used to Calculate Seismic Fragility Curves.”. Center for Nuclear Waste Regulatory Analyses. <https://www.nrc.gov/docs/ML1712/ML1712A268.pdf>

The figure below shows one of the fragility curves developed in the paper.

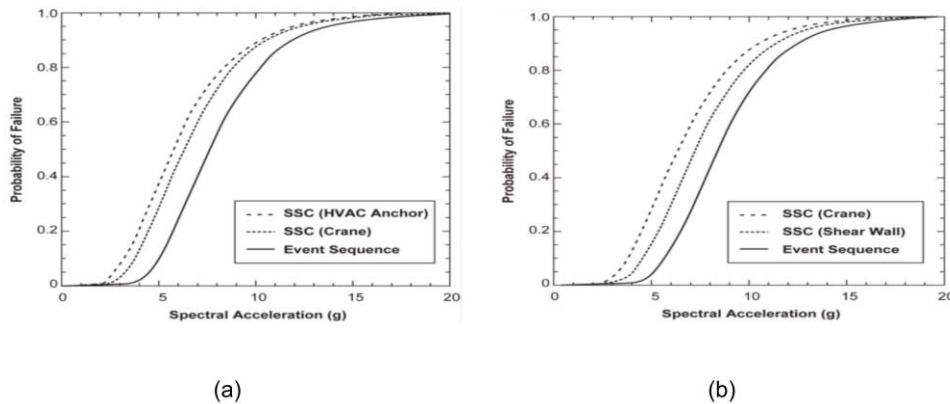


Figure 31. Hypothetical fragility curves for individual and combined fragility for: (a) event sequence 3 and (b) event sequence 4. Source: B Dasgupta.2017.

4.10 Electric Substations

Zekavati et al. (2022)¹ used risk assessment based on reliability methods to evaluate the anticipated yearly loss from seismic hazards to an electric substation. To conduct the study, Zekavati et al. (2022) developed a model based on the Pacific Earthquake Engineering Research Center’s general approach for earthquake vulnerability evaluation and employed scenario sampling that produce yearly random samples of seismic activities and their impacts. To simulate seismic hazards and the destruction level of substations, the authors developed probabilistic models relying on fragility functions and repair costs. The economic loss or repair cost of substations is calculated through a probabilistic approach that includes past earthquake damages. The paper remarks that the proposed model is applied to an area that comprises 92 substations whose voltage levels are 400, 230, and 62 kV.

Remarks: The intensity measure used is point ground acceleration. The figure below shows multiple fragility curves developed for substations.

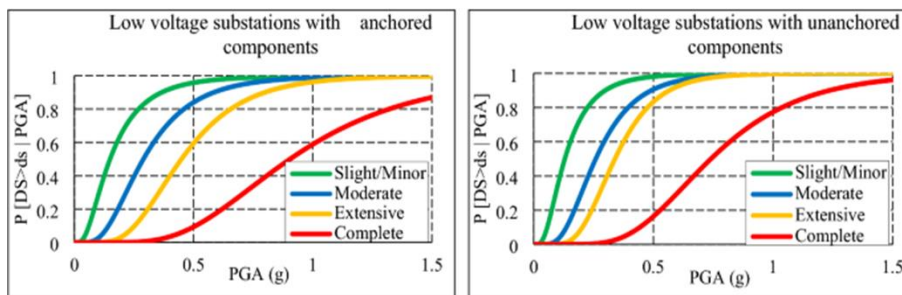


Figure 32. Fragility functions for substations with anchored and unanchored components Source: A A Zekavati, M A Jafari, A Mahmoudi. 2021.

¹ A A Zekavati, M A Jafari, A Mahmoudi. 2021. “Regional seismic risk assessment method for electric power substations: a case study”. Life Cycle Reliability and Safety Engineering. 11 (2022) 105115. <https://link.springer.com/article/10.1007/s41872-021-00178-9>

4.11 Urban Gas Pipelines

Farahani et al. (2020)¹ assess the earthquake vulnerability of the Asaluyeh city urban gas distribution system by investigating all geo-seismic threats using the HAZUS approach. The document examines the ignition caused by the earthquake by using the fault tree method and evaluates the impacts of the seismic event using the PHAST package. The paper also evaluates the gas distribution system damage risk, humanitarian risk and economic risks.

Remarks: The intensity measure used is peak ground acceleration. Multiple equations are listed in the paper, among which the following one represents the relationship between peak ground velocity and repair rate.

$$R.R = 0.00003 \times PGV^{2.25} \quad (25)$$

The study assumed that the power distribution network is the spark source that can cause an ignition in case of the gas pipeline failure due to seismic events. For that reason, the paper presents the graph below, which shows the link between the vulnerability of power networks and various levels of failure.

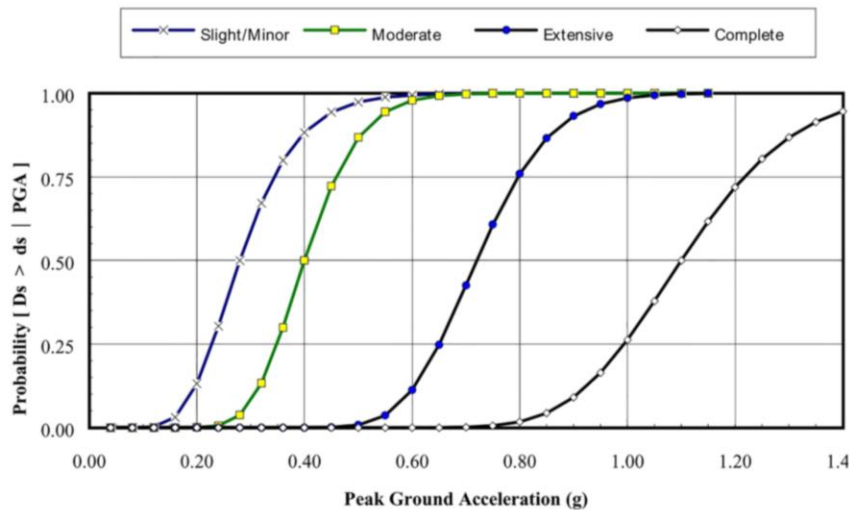


Figure 33. Fragility curves for electric power lines according to failure levels to a seismic event
 Source: S Farahani, A Tahershamsi, B Beham. 2020.

¹ S Farahani, A Tahershamsi, B Beham. 2020. "Earthquake and Post-earthquake Vulnerability Assessment of Urban Gas Pipelines Network." *Natural Hazards* 100(301).
<https://link.springer.com/article/10.1007/s11069-020-03874-4>

4.12 Oil Pumping Station

Urlainis and Shohet (2022)¹ propose a method for developing exclusive fragility curves that is based on decomposing a critical infrastructure into its main pieces and determining the different failure mechanisms of the infrastructure. To determine the fragility parameters, the authors conducted a failure assessment for each damage state through a Fault Tree Analysis and estimated the parameters with respect to the rate of exceedance. Urlainis and Shohet (2022) applied their proposed approach to an oil pumping station case study where three alternatives of a pumping station are considered. The alternative of the oil pumping station varied by the subcomponents used in each case. The paper notes that changing subcomponents has an impact on the estimated values of the fragility parameters.

Remarks: The intensity measure used is peak ground acceleration. The research uses R squared as the proposed fit test when the Sum Square Error is computed as followed

$$SSE_i = \sum_{m=1}^{N_{IM}} \left[P_{m,i} - \left(\frac{\ln (IM_m / \theta'_{ds_i})}{\beta'} \right) \right] \quad (26)$$

Where SSE = Sum of Squares Error

IM = uncertain excitation, ground motion intensity measure (PGA, PGD, PGV)

θ'_{ds_i} = new median capacity for each damage state

i = damage state

β' = new logarithmic standard deviation

The figure below displays fragility curves' graph based on parameters determined from the equation above.

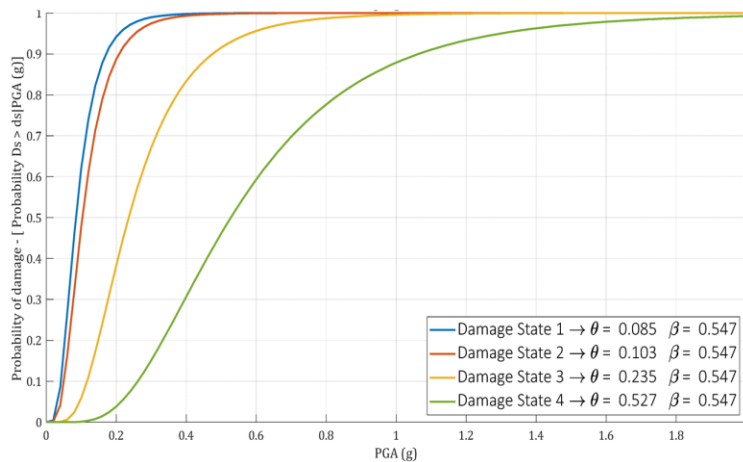


Figure 34. Exclusive fragility curves and parameters for an oil pumping stations

Source: A Urlainis, I M Shohet. 2022.

¹ A Urlainis, I M Shohet. 2022. "Development of Exclusive Seismic Fragility Curves for Critical Infrastructure: An Oil Pumping Station Case Study". Buildings 12-6 (2022) 842. <https://doi.org/10.3390/buildings12060842>

5.0 Ice Loads

5.1 Transmission Towers

Rezaei et al. (2015)¹ use the notion of statistical learning theory to develop a probabilistic framework for vulnerability evaluation of electric transmission towers under unbalanced ice loads. Concerning the statistical learning theory, the authors substituted each component's implicit limit state function with an estimated polynomial function that possesses good prediction properties.

The study outcomes are conveyed in the form of fragility curves for 3 distinct unbalanced loading cases of transverse, longitudinal, and torsional loadings. Additionally, the paper examines the impact of different design specifications, such as icing location and rate, wind direction and speed, and location of ice accumulation on the fragility curves of towers.

Remarks: Ice load is expressed in terms of ice thickness in millimeters (mm). Pages 3 and 5 display a few mathematical expressions, among which the following one is an equation representing the analytical generalization path for model selection adopted from Cherkassy et al., 1999, Vapnik, 1995.

$$R(w) = R_{emp}(w) \cdot \left(1 - \sqrt{p - p \ln p + \frac{\ln n}{2n}} \right)^{-1} \quad (27)$$

Where $R(w)$ = unknown prediction error.

$R_{emp}(w)$ = known empirical error

n = number of training samples

p = ratio of VC dimension (h) to the sample size

The figure below gives a visual representation of the fragility curve of the tension tower under ice hazard.

¹ S N Rezaei, L Chouinard, F Legeron, S Langlois. 2015. "Vulnerability analysis of transmission towers subjected to unbalanced ice loads." International Conference on Applications of Statistics and Probability in Civil Engineering (ICASP) (12th :2015) <https://dx.doi.org/10.14288/1.0076203>

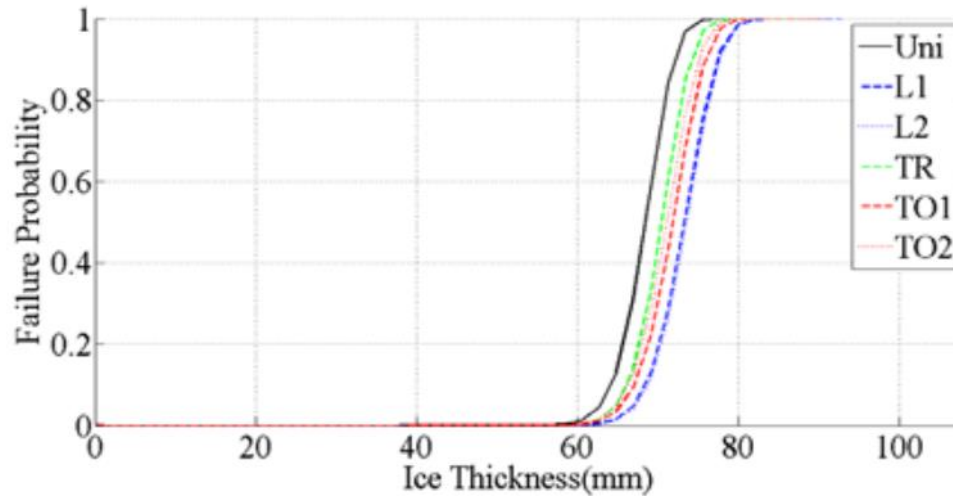


Figure 35. Fragility curves for tension tower 3 under different scenarios of ice loading with no wind

Source: S N Rezaei, L Chouinard, F Legeron, S Langlois. 2015.

6.0 Flood

6.1 Buildings

Nofal et al. (2020)¹ propose a multi-variate and single-variable component-based flood fragility model. According to the paper, this model solves the issues of incorporating uncertainties in flood damage functions caused by the lack of flood-related data and the nature of the deterministic models often used for this purpose. The article highlights that the proposed method relies on expert-approved data retrieved from online sources. A Monte Carlo simulation is used to apply uncertainties to the data before a component fragility function is used to develop loss functions. Nofal et al. (2020) point out that the specificity of their work is that it provides a framework for developing flood fragility functions for buildings without conducting an empirical study.

Remarks: The intensity measures used in this study are water depth and duration. Depth is expressed in meters, m, and duration in hours, hr.

Mathematical functions can be found on pages 2, 4, 9. The following fragility equation is a lognormal cumulative distribution function for components and structural systems.

$$F_r(x) = \Phi \left[\frac{\ln(x) - \lambda_R}{\xi_R} \right] \quad (28)$$

Where $F_R(x)$ = fragility function,

$\Phi[.]$ = standard normal cumulative distribution function,

λ_R = logarithmic median of resistance R

ξ_R = logarithmic standard deviation of resistance R

The figure below show an example of fragility curve developed for building components such as AC unit and an electrical outlet.

¹ O M Nofal, J W Van de Lindt, T Q Do. 2020. "Multi-variate and single-variable flood fragility and loss approaches for buildings" Reliability Engineering & System Safety 202 (2020) 106971. <https://doi.org/10.1016/j.ress.2020.106971>

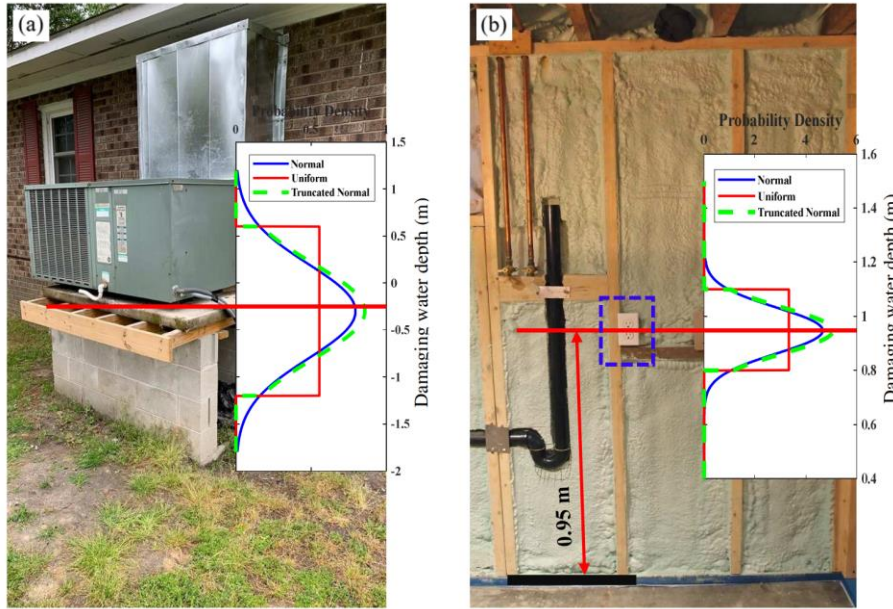


Figure 36. Damaging water depth using a truncated normal for a (a) External AC unit; (b) Electrical outlet.

Source: O M Nofal, J W Van de lindt, TQ Do.2020.

6.2 Electrical Component

Espinoza et al. (2016)¹ recommend a multi-phase resilience analysis method that can evaluate any natural threat that can potentially cause severe multiple or single damage to important infrastructures such as electric power networks. The multi-phase resilience framework consists of four steps: threat characterization, risk evaluation of the system’s elements, system’s reaction, and system’s restoration. The paper mentions that the entire process is time-dependent and necessitates multidisciplinary work. A case study is performed on a reduced format of Great Britain’s power system subjected to windstorms and floods.

Remarks: The intensity measures used are wind speed expressed in meters per second (m/s) for wind hazards and flood depth expressed in millimeters for flood hazards (mm). The equation below shows how rainfall parameters are computed

$$\pi(\gamma, \rho, \lambda) = \frac{T(\lambda - year)}{P(\gamma, \rho)}, \text{ for } \gamma \in [1979, \dots, 2011] \quad (29)$$

Where $\pi(\gamma, \rho, \lambda)$ = scale parameter,
 λ -year = return period,
 γ = year,
 ρ = region
 $T(\lambda - year)$ = return value

¹ S Espinoza, M Panteli, P Mancarella, H Rudnick. 2016. “Multi-phase assessment and adaptation of power systems resilience to natural hazards”. Electric Power Systems Research 136 (2016) 352-361. <https://doi.org/10.1016/j.epsr.2016.03.019>

The graph below is an example fragility curve displayed in the paper

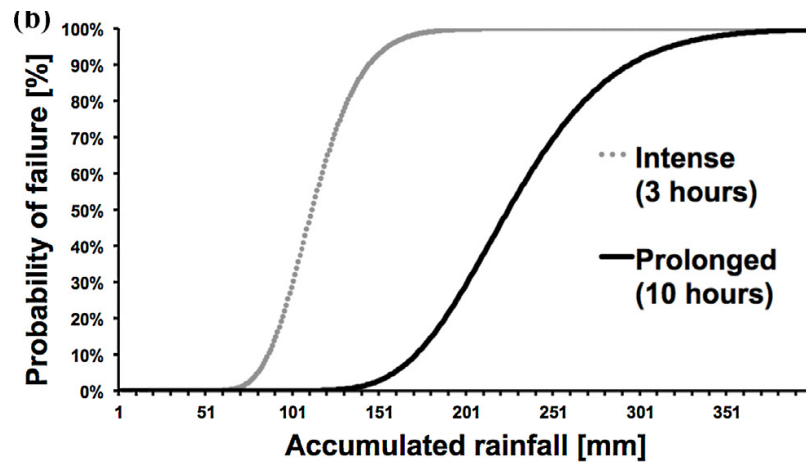


Figure 37. Fragility function for electrical components with respect to amount of rainfall
Source: S Espinoza, M Panteli, P Mancarella, H Rudnick. 2016.

6.3 Electric Components

Chen, Bo's 2020¹ project consisted of developing an optimization method to facilitate the integration of distributed solar energy in resilience amelioration of distribution grid against ravaging weather conditions and guarantee a 5-day islanded operation backed by distributed energy resources. Out of the six tasks around which the project is organized, task 4 is the one that consists of creating test cases for pre-event preparation and post-event operation optimization solution models. Part of task 4 pertains to developing fragility curves for electric parts under flood and wind hazards.

Remark: The paper shows two fragility curve graphs based on flood and windstorm. The figure below graphically portrays the relationship between food depth and select electric components.

¹ B Chen. 2020. "Optimization framework for solar energy integrated resilient distribution grid." Argonne National Laboratory CPS#34228- Final Project Review. http://wzy.ece.iastate.edu/project/34228_FPR-ANL_v0.4.pdf

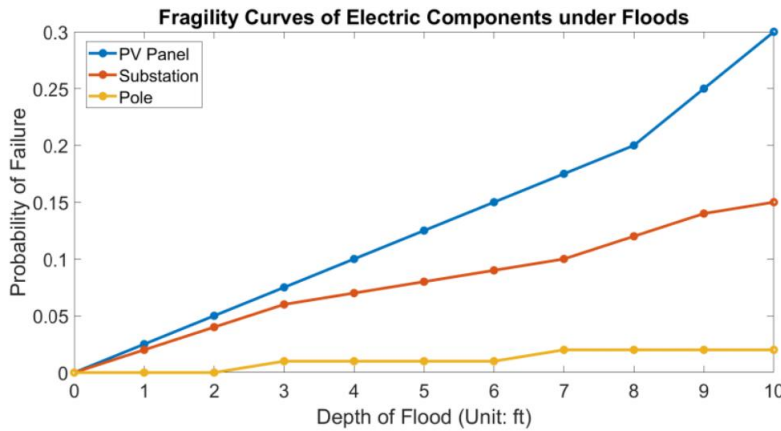


Figure 38. Fragility curves of electric components based on flood depth
 Source: B Chen. 2020.

6.4 Electrical Grid

Sanchez-Munoz et al. (2020)¹ recommend a methodology based on a probabilistic approach that permits the study of a flood hazard map to estimate the failure probability of electrical equipment and their potential consequences. On the other hand, the paper defines a monetization method for the consequences determined based on the estimated failure risk. The presented method is applied to two case study cities which are Bristol, UK and Barcelona, Spain. The article mentions that the two essential inputs indispensable to the case studies were: accurate GIS hazard flooding models and the area where the electrical equipment are located. However, a variety of other variables, such as water depths, fragility, and damage curves, were necessary to assess and monetize the flood hazard.

Remarks: The intensity measure used is flood depth expressed in meters. The water depth was calculated per location following the equation below:

$$WDA = \frac{1}{n} \sum_{i=1}^n Y_i \quad (30)$$

Where: WDA = Water Depth Average
 Y_i is the probability of failure

The figure below represents the fragility curves developed in the paper for various electrical substations and distribution facilities.

¹ D Sánchez-Muñoz, J L Domínguez-García , E Martínez-Gomariz, B Russo, J Stevens, and M Pardo. 2020. "Electrical Grid Risk Assessment Against Flooding in Barcelona and Bristol Cities" Sustainability 12- 4(2020) 1527.. <https://doi.org/10.3390/su12041527>

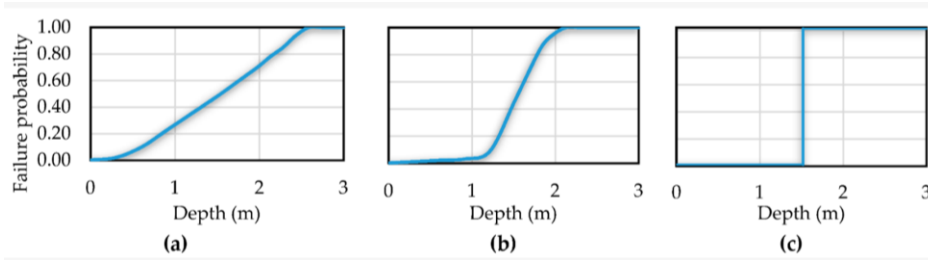


Figure 39. Flooding fragility curves for high voltage, medium voltage and low voltage substations and distribution centers

Source: D Sánchez-Muñoz, et al 2020.

6.5 Power Grid

Karagiannis et al. (2017)¹ mainly focused on crafting a methodology to examine the effect of climate change on the risk created by floods to critical infrastructure, such as power grids. The authors specifically focused on understanding how losses for a 100-year flood scheme change if certain factors such as infrastructure effects beyond the flood zone, are accounted for. They also examined the impact of climate change on future risk rates and carried out a case study on a power network located in a major urban center in Western Europe. Karagiannis et al. (2017) highlight that their approach incorporates a future prediction of the occurrence interval of designated flood scenarios and the evaluations of the quantified losses sustained by critical infrastructures.

Remarks: The scope of the study is limited to demonstrating the applicability of the proposed methodology and to derive initial conclusions concerning the effects of floods on critical facilities.

The equation below is a formula for monetizing losses due to floods:

$$Flood\ Cost\ (FC) = \frac{GDP \cdot t_f \cdot P_f}{365 \cdot P_{tot}} \quad (31)$$

Where GDP = Gross Domestic Product of the jurisdiction under review

T_f = the estimated duration of the flood episode (in days).

P_f = the population in the inundated area, estimated by the combination of the area with a population density map.

P_{tot} = the jurisdiction's entire population.

The figure below shows a flood damage graph used in the paper. It is built from flood model of HAZUS®-MH.

¹ G M Karagiannis, Z I Turksezer, L Alfieri, L Feyen, E Krausmann. 2017. "Climate change and critical infrastructure-floods". Floods, EUR 28855 EN, Publications Office of the European Union, Luxembourg 2017. https://www.researchgate.net/publication/322024183_Climate_Change_and_Critical_Infrastructure_-_Floods

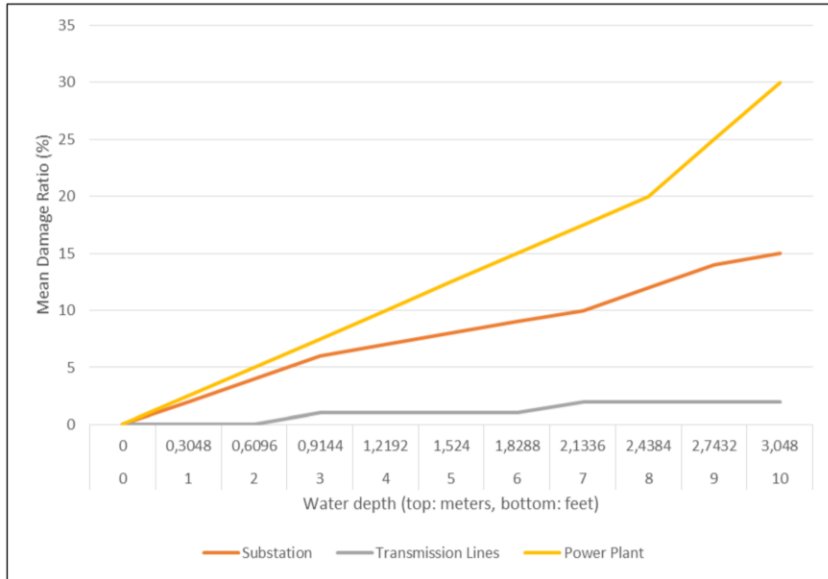


Figure 40. Mean damage ratio for substations, transmission lines and power plants
 Source: HAZUS®-MH G M Karagiannis, Z I Turksezer, L Alfieri, L Feyen, E Krausmann. 2017.

7.0 Tsunami

7.1 Utility Pole

Williams et al. (2020)¹ present a study that partly evaluates the tsunami risk for utility poles damaged during the 2018 Sulawesi Tsunami in Indonesia. The researchers carried out a field survey and collected remotely sensed data to build a dataset later used to develop tsunami fragility functions for utility poles and roads. The paper reveals that the data collected through field survey is expanded through satellite and “street view” imageries of the utility poles before and after the tsunami. The authors claim that the combination of field and satellite data leads to a higher-quality dataset. They compared three surface interpolation models with the natural neighbor method to produce high-quality visual correlation and statistical survey of inundation depths.

Remarks: The intensity measure used is inundation depth in meters, m. The fragility function model used in the study is based on cumulative link models and represents the relationship between a tsunami and assets damage.

$$P(DS \geq ds | HIM) = \Phi(\hat{\beta}_j + \hat{\beta}_2 \ln(HIM)) \quad (32)$$

Where DS = damage state

$\hat{\beta}_j$ = intercept

$\hat{\beta}_2$ = slope

HIM = hazard intensity measure (e.g inundation depth)

The graph below is a visual display of the fragility curve of utility poles.

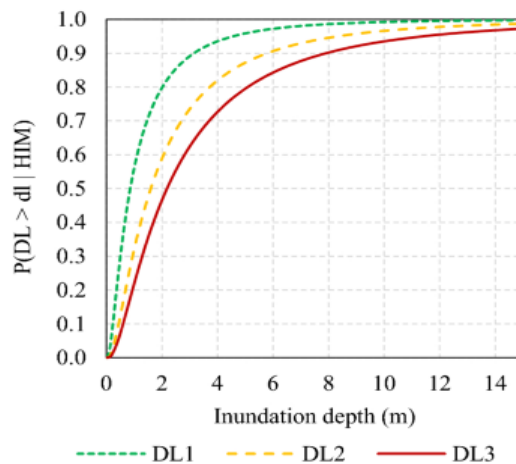


Figure 41. Water depth damage fragility functions for mixed utility poles. Source: J Williams et al 2020.

¹ J Williams, R Paulik, T Wilson, L Wotherspoon., A Rusdin, G M Pratama. 2020. “Tsunami Fragility Functions for Road and Utility Pole Assets Using Field Survey and Remotely Sensed Data from the 2018 Sulawesi Tsunami, Palu, Indonesia”. Pure and Applied Geophysics 177-8 (2020). <https://link.springer.com/article/10.1007/s00024-020-02545-6>

8.0 Volcanic

8.1 Water Treatment Site

Wilson et al. (2017)¹ introduce a methodology for using fragility and vulnerability functions to express the relationship between hazard intensity and volcanic impact. The framework of the study considers various impact intensity measurements, impact data sources, uncertainty evaluation, and data fitting. Post-eruption impact evaluations constitute the primary data sources used in the study. However, they are complemented by laboratory tests and expert judgment based on previously conducted studies. The proposed framework is applied to various critical infrastructures, including water supply, electricity supply, and transport systems.

Remarks: The intensity measure is tephra expressed in millimeters. The following equation displays the piecewise linear equation used to compute the probability of impact state during a volcanic eruption

$$P(IS \geq IS_i) = \begin{cases} 0 & HIM = 0 \\ m_{1,i}HIM + c_{1,i} & k_1 < HIM \leq k_2 \\ m_{2,i}HIM + c_{2,i} & k_2 < HIM \leq k_3 \\ m_{3,i}HIM + c_{3,i} & k_3 > HIM \end{cases} \quad (33)$$

Where $m_{1,i}$, $m_{2,i}$, $m_{3,i}$: slope constants

$c_{1,i}$, $c_{2,i}$, $c_{3,i}$: intercept constants for 3 linear segments for the i -th impact state.

k_1 , k_2 , k_3 : are constant and $k_1 \neq k_2 \neq k_3$. they are the critical HIM values for which various linear segments apply.

The paper presents fragility functions for various infrastructures such as electric substations, and transmission lines. However, the figure below displays the fragility curve for a water treatment facility.

¹ G Wilson, T M Wilson, N I Deligne, D M Blake, J W Cole. 2017. "Framework for developing volcanic fragility and vulnerability functions for critical infrastructure". Applied Volcanology 6-14(2017). <https://doi.org/10.1186/s13617-017-0065-6>

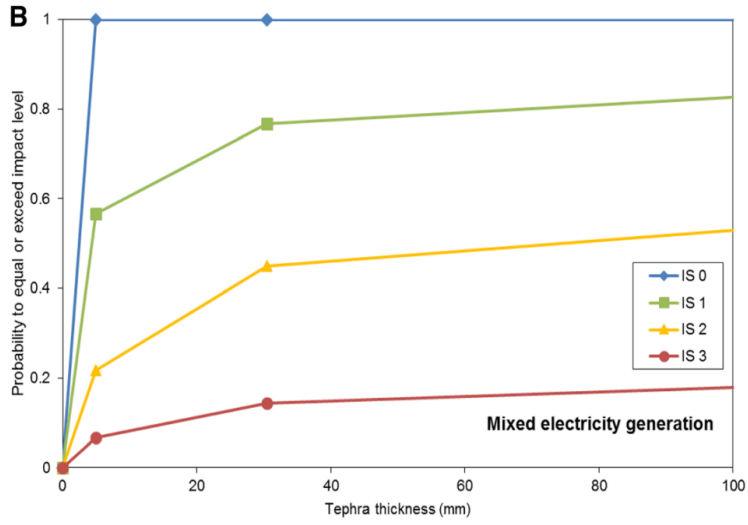


Figure 42. Derived fragility functions for a water supply treatment plant
 Source: G Wilson et al 2017

9.0 Geomagnetic Storms

9.1 Power Grid

Kappenman’s (2010)¹ report relates the danger of geomagnetic storms on the Earth occasioned by solar activity. The report also explains their past and future impacts on the U.S power grid installations. Using the ability to model the effects of the geomagnetic fields on the power grids, Kappenman draws from the understanding of past events to forecast the potential impacts of future geomagnetic storms. He clarifies that the document’s main purpose is to provide a foundation for making future suggestions for protecting the U.S. power grid from geomagnetic threats.

The first section of the report discusses how geomagnetic storms impact the power system, while the second section focuses on the damages caused by the March 13, 1989, Great Geomagnetic Storm in the United States and Canada. The third section is a projection of future and potential storm events; however, the last section provides details on the impacts on vulnerable EHV transformers in the U.S. The document includes appendices that offer supportive information to the analysis developed in the body of the report.

Remarks: The geomagnetic storm is measured in nanoteslas per minute, nT/min. The graph below is found in Appendix 1 and illustrates a power grid failure probability due to geomagnetically induced current.

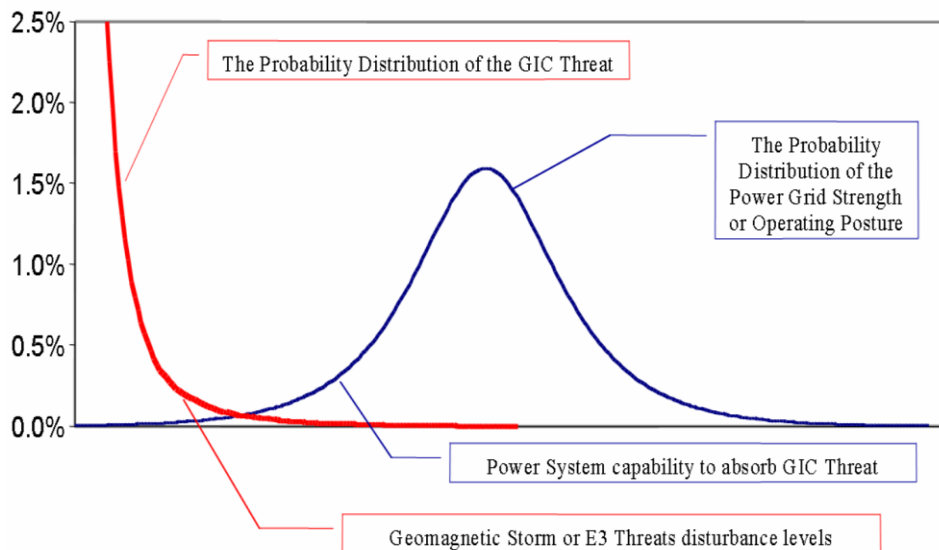


Figure 43. Power grid failure probability analysis from GIC threat scenario. Source: J Kappenman. 2010.

¹ Source: J Kappenman. 2010. “Geomagnetic Storms and Their Impacts on the U.S. Power Grid”. Metatech. <https://irp.fas.org/eprint/geomag.pdf>

10.0 Heat

10.1 Distribution Transformers

Csanyi's, Edvard 2021¹ article reviews the most prevalent failure patterns of electrical equipment in distribution networks. This paper is not based on a modeling or empirical study; rather, it describes different hazards that can damage certain components of a given power grid. Csanyi relates that hot temperature can cause a transformer's loss of life because it damages the insulation polymers that protect the equipment. According to the article, a standard transformer is built for hot spot temperatures of either 110 degrees Celsius or 95 degrees Celsius (55 degrees Celsius rise insulation), however hot spots drastically reduce the life of a transformer. The other electrical power system components discussed in the article are underground cables, overhead lines, circuit breakers, insulators and bushing, and surge arresters.

Remarks: Given that a transformer's life decreases significantly with the damage of its insulators, the paper shows how to calculate the insulation life using the equation below.

$$\text{insulation life} = 10^{(K1/(273 + ^\circ\text{C})) + K2} \text{ hours} \quad (34)$$

The constants for the equation were experimentally calculated for both distribution and power transformers. More information about the constants are given as transformers loading guide.

The figure below shows the insulation half-life in relationship to hot spot.

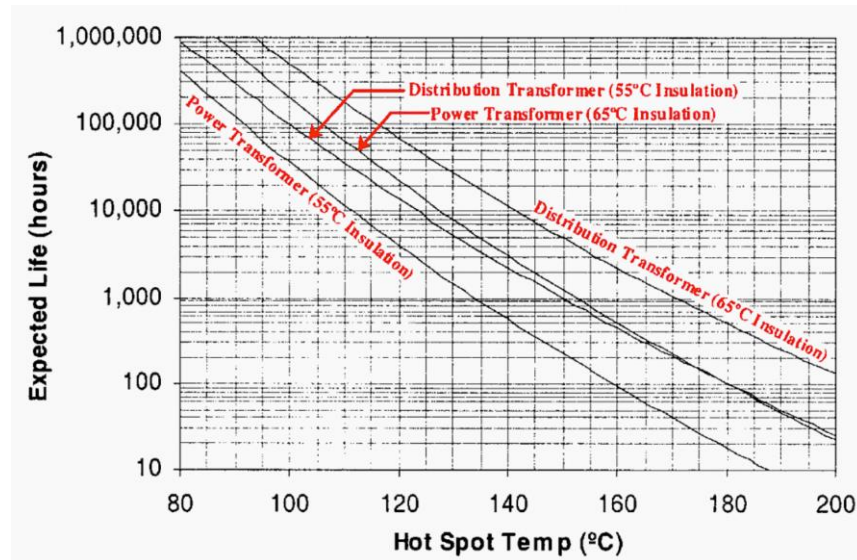


Figure 44. Expected insulation half-life of transformers as a function of hot spot temperature. Source: Csanyi, Edvard. 2021.

¹ Edvard, Csanyi. 2021. "The most common failure modes of electrical equipment in distribution systems." Electrical Engineering Portal. <https://electrical-engineering-portal.com/failure-modes-electrical-equipment-distribution-systems>

11.0 Tornado

11.1 School Building

Wang and Van de Lindt 2022¹ propose a set of design mixture of a fortified masonry school building with various performance objectives with the goal to enable schools to reopen faster after a tornado event. Based on the latest tornado chapter in ASCE 7-22, the authors developed tornado fragility curves for a specified school edifice with upgraded designs. The fragility analysis was conducted through a Monte Carlo Simulation. The authors incorporated the school with improved design into a community level model with school attendance areas to evaluate the effect of improved school design on enabling a quicker return to classes after a tornado. The study concludes that the improved design led to less damage and had a significant impact on maintaining educational continuity.

Remarks: The intensity measure used in wind speed and is expressed in miles per hour (mph). In the report, the following equation is used to calculate the design wind pressures for buildings of all height.

$$p = qGC_p - q_i(GC_{pi}) \left(\frac{lb}{ft^2}\right) \left(\frac{N}{m^2}\right) \quad (35)$$

Where GC_p = external pressure coefficient
 GC_{pi} = internal pressure coefficient

The figure below shows the fragility curve of school building subject to different damage levels.

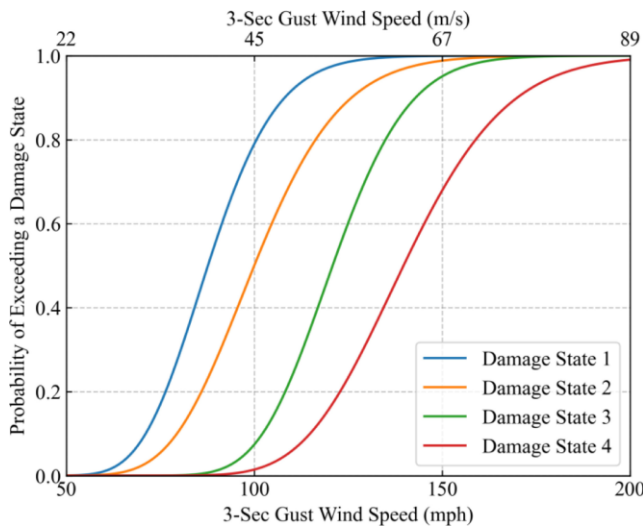


Figure 45. School fragility curve using Design level 2. Source: W (L) Wang, J W van de Lindt. 2022.

¹ W (L) Wang, J W van de Lindt. 2022. "Quantifying the effect of improved school and residential building codes for tornadoes in community resilience." Resilient Cities and Structures 1-1(2022) 65-79. <https://doi.org/10.1016/j.rcns.2022.04.001>

11.2 Residential Building

Wang and van de Lindt 2021¹ promote a model based on a multi-layer *Monte Carlo* simulation to devise a two-stage recovery strategy for residential buildings. The first stage concerns the functional downtime caused by delay and the second stage pertains to functional downtime caused by repair. According to the paper, the delay aspect of the model was adjusted based on the REDI framework and covers the obstructing factors that retard repairs, such as insurance claims, damage inspection, and building authorizations. Also, the study accounted for financing delays by examining households' incomes. The repair part of the proposed model is based on the FEMA P-58 framework approach and verified through fragility functions. Wang and van de Lindt investigated multiple policies to examine the case of the 2011 Joplin tornado event. In conclusion the article defends that the presented model can effectively contribute to the recovery process.

Remarks: Multiple equations are listed on the paper on pages 2, 3, and 4. The equation below represents the estimated delay time for financing. The authors note that the time delay estimates only applicable to U.S.

$$T_{FINA,ij} = \sum_{n=1}^4 P[T_{n,ij}] \cdot T_{n,ij} \quad (36)$$

Where n = refers to four funding options

i, and j represents each realization in the Monte Carlo simulation and identification of building itself, respectively.

$P[T_{n,ij}]$ = probability of the households to access one financial option

$T_{n,ij}$ = estimated time obtained from cumulative lognormal functions

The figure below is a graphical representation of the fragility curve of wooden building subjected to tornado hazard. The intensity measure used is wind speed expressed in meter per second.

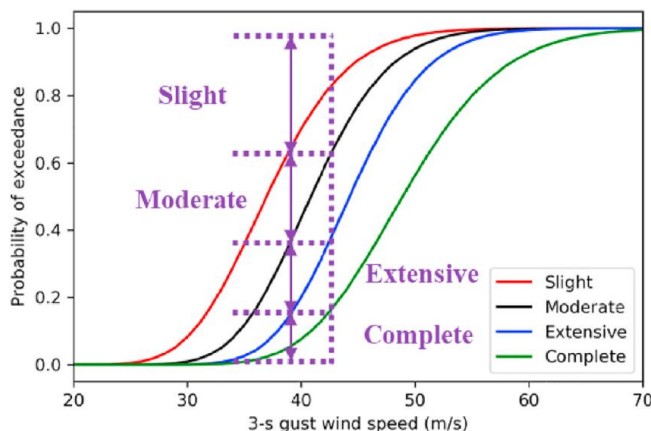


Figure 46. Fragility curve of a wood-frame residential building due to tornado
Source: W (L) Wang, J W van de Lindt. 2021.

¹ W (L) Wang, J W van de Lindt. 2021. "Quantitative modeling of residential building disaster recovery and effects of pre- and post-event policies." *International Journal of Disaster Risk Reduction* 59 (2021) 102259. <https://doi.org/10.1016/j.ijdrr.2021.102259>

12.0 Power Outage

12.1 Manufacturing Plant

Ericson and Lisell (2020)¹ devised a flexible framework for quantifying the cost of power blackouts for a range of consumer categories and blackout lengths. The paper begins by classifying costs into variable flow costs, variable stock costs, and fixed expenses. Then, it develops functional models from each cost category to produce parameterized functions that are used to evaluate outage costs. Ericson and Lisell (2020) claim that their model is more realistic than the commonly used economic model, offers increased flexibility, and is less data dependent. The authors also remark that the proposed model enables the quantification of outage costs for different timeframes and that it can be adjusted to factor in multiple data availability and load types.

Remarks: The model is applied to a manufacturing plant and a fire station in the paper. The loss function used in the paper is modeled as a Weibull distribution expressed as followed:

$$L_i(t) = yi(0) \left[\left(\frac{k}{\lambda} \right) \left(\frac{\bar{t}}{\lambda} \right)^{k-1} \exp \left(- \left(\frac{\bar{t}}{\lambda} \right)^k \right) \right] \quad (37)$$

Where k and λ = capture the form of the distribution
 \bar{t} = possibility of shifting distribution to factor in the fact that time may go by before any stock spoils
 y = total dollar value of perishable stock.

The figure below shows blackout costs for an illustrative manufacturing plant

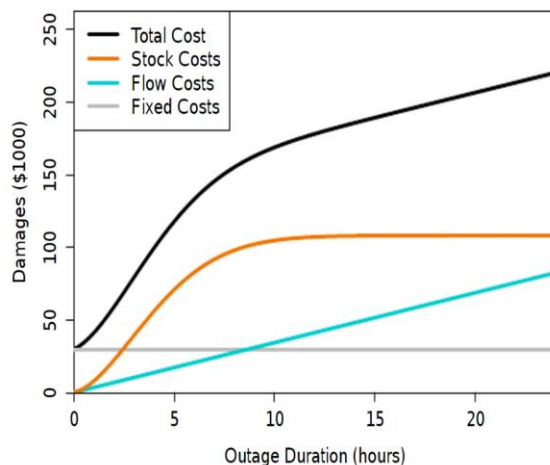


Figure 47. Total cost curves for manufacturing plant based on duration of outage
 Source: S Ericson, L Lisell. 2020.

¹ S Ericson, L Lisell. 2020. "A flexible framework for modeling customer damage functions for power outages". Energy systems 11-3(2020) 1-17. <https://link.springer.com/article/10.1007/s12667-018-0314-8>

12.2 Health Care

Mechtenberg et al. (2020)¹ devised two methodologies to estimate the hidden costs incurred by healthcare systems due to power outages. To create the first methodology, the authors examined research literature and existing measurement methods to gather data regarding hourly energy outages for different energy healthcare system (EHS) categories in Iraq, Ghana, Bangladesh, and Uganda. In the study, the EHS in Iraq uses SolarPV; in Ghana, it uses Hydroelectric; in Bangladesh, it uses SolarPV and Wind; whereas in Uganda, it uses Diesel and Grid power. The second methodology concerns the estimation of patient risks based on medical procedures and the length and time of electricity failure. The two methodologies are later combined to derive the hidden costs caused by electricity outage as the quotient of the Value of Statistical Lives and Energy shortage. The authors then compared hidden costs to traditional energy costs and found that hidden costs are significantly higher.

Remarks: Electricity failure duration is measured in hours. The graph below displays the risks of beginning a medical procedure after which an energy outage occurs. No mathematical equation is given in the paper.

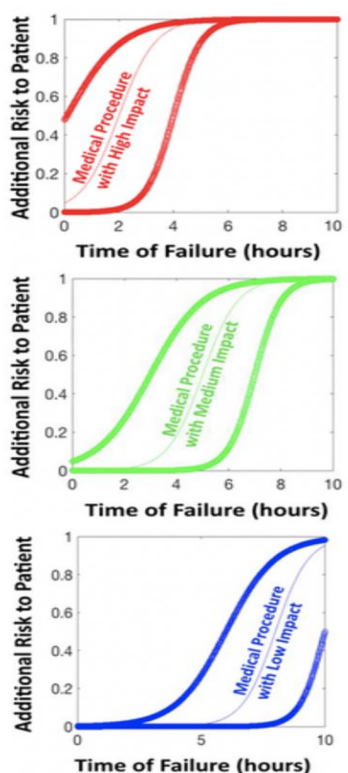


Figure 48. Additional risk to patient due loss of electricity during a medical procedure that requires an electric medical device.

Source: Mechtenberg et al 2020.

¹ A Mechtenberg, B Mclaughlin, M DiGaetano, A Awodele, L Omeeboh, E Etwalu, et al. 2020. "Health care during electricity failure: The hidden costs". Plos ONE 15-11 (2020). <https://doi.org/10.1371/journal.pone.0235760>

12.3 Industrial Customers

Yoshida and Matsushashi (2013)¹ estimate the power outage cost of factories in Japan by surveying over 5000 manufacturing plants categorized as energy management factories. They fitted a distribution function to sample data before estimating the median unit cost of electricity failure. The authors preferred to use the estimated median instead of the sample one because the median derived from the estimation is less impacted by randomness. A bootstrap method is used to estimate the confidence interval of the median. At the same time, the Weibull and the log-logistic distribution are employed as potential distribution functions of the unit cost of electricity blackouts. The result of the study shows that the median unit cost incurred by factories is 672 yen/kWh.

Remarks: The log-logistic distribution used to calculate the probability $P(T)$ that the unit cost exceeds a certain amount of T yen is expressed as follow:

$$P(T) = 1 / (1 + \exp(a + b \log(T))) \quad (38)$$

Where a and $b = \text{constant}$
Median $M[T] = \exp(-a/b)$

The figure below shows the regressions obtained by the Weibull and log-logistic distributions.

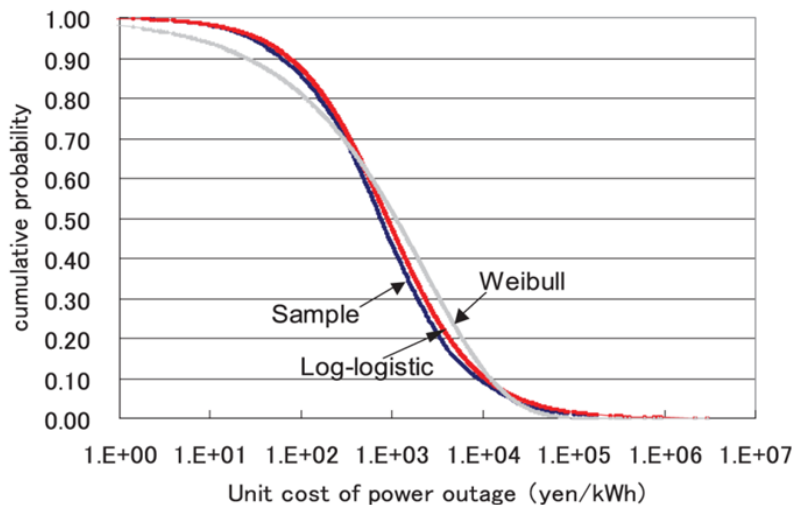


Figure 49. Probability of unit costs due to a power outage.
Source: Y Yoshida, R Matsushashi. 2013.

¹ Y Yoshida, R Matsushashi. 2013. Estimating Power Outage Costs Based on a Survey of Industrial Customers. *Electrical Engineering in Japan* 185-4 (2013).
<https://onlinelibrary.wiley.com/doi/pdf/10.1002/eej.22306>

13.0 References

- Alam, MS, BG Simpson, AR Barbosa, MJ Olsen. No date. Fragility Function Viewer. CLiP Lifelines Fragility Database v 0.1.0. School of Civil & Construction Engineering. Oregon State University. <https://clip.engr.oregonstate.edu/CLiPFragilityDatabase/>
- Alam, MS, BG Simpson, AR Barbosa. 2020. Defining Appropriate Fragility Functions for Oregon. A report for the Cascadia Lifeline Program. School of Civil and Construction Engineering. Oregon State University. <https://app.box.com/s/vkq345sz5rvyd49k9nnjhvu907fqnkb8>
- Allen-Dumas, MR, Binita KC, CI Cunliff. 2019. "Extreme Weather and Climate Vulnerabilities of the Electric Grid: A Summary of Environmental Sensitivity Quantification Methods." ORNL/TM-2019-1252. <https://www.energy.gov/sites/prod/files/2019/09/f67/Oak%20Ridge%20National%20Laboratory%20EIS%20Response.pdf>
- Baghmisheh, AG, M Mahsuli. 2021. "Seismic performance and fragility analysis of power distribution concrete poles". Soil Dynamics and Earthquake Engineering 150(2021)106909. <https://doi.org/10.1016/j.soildyn.2021.106909>
- Bennett, JA, CN Trevisan, JF DeCarolis, C Ortiz-García, M Pérez-Lugo, BT Etienne, AF Clarens. 2021. "Extending energy system modelling to include extreme weather risks and application to hurricane events in Puerto Rico. Nat Energy 6 (2021) 240-249. <https://doi.org/10.1038/s41560-020-00758-6>
- Bilionis, DV, D Vamvatsikos. 2019. "Wind performance assessment of telecommunication towers: A case study in Greece." Eccomas Procedia COMPDYN (2019) 5741-5755. DOI: <https://files.eccomasproceedia.org/papers/compdyn-2019/19629.pdf?mtime=20191121000158>
- Cavaliere, F, P Franchin, PE Pinto. 2014. "Fragility Functions of Electric Power Stations". In: Pitilakis, K., Crowley, H., Kaynia, A. (eds) SYNER-G: Typology Definition and Fragility Functions for Physical Elements at Seismic Risk. Geotechnical, Geological and Earthquake Engineering, vol 27. Springer, Dordrecht. https://doi.org/10.1007/978-94-007-7872-6_6
- Ceferino, L, N Lin, D Xi. 2021. "Stochastic Modeling of Solar Generation During Hurricanes." PREPRINT (Version 1) available at Research Square <https://doi.org/10.21203/rs.3.rs-797974/v1>
- Csanyi, E. 2021. "The most common failure modes of electrical equipment in distribution systems." Electrical Engineering Portal. <https://electrical-engineering-portal.com/failure-modes-electrical-equipment-distribution-systems>
- Dasgupta, B. 2017. "Evaluation of Methods Used to Calculate Seismic Fragility Curves". Center for Nuclear Waste Regulatory Analyses. <https://www.nrc.gov/docs/ML1712/ML17122A268.pdf>

- Dinh, NH, J-Y Kim, SJ Lee, KK Choi. 2019. "Seismic Vulnerability Assessment of Hybrid Mold Transformer Based on Dynamic Analyses". 2019. Applied Sciences 9-15(2019) 3180. <https://doi.org/10.3390/app9153180>
- Ericson, S, L Lisell. 2020. "A flexible framework for modeling customer damage functions for power outages". Energy systems 11-3(2020) 1-17. <https://link.springer.com/article/10.1007/s12667-018-0314-8>
- Farahani, S, A Tahershamsi, B Beham. 2020. "Earthquake and Post-earthquake Vulnerability Assessment of Urban Gas Pipelines Network." Natural Hazards 100(301). <https://link.springer.com/article/10.1007/s11069-020-03874-4>
- Fu, X, HN Li, L Tian, J Wang. 2019. "Fragility Analysis of Transmission Line Subjected to Wind Loading." Journal of Performance of Constructed Facilities 33-4(2019). <https://ascelibrary.org/doi/10.1061/%28ASCE%29CF.1943-5509.0001311>
- Espinoza, S, M Panteli, P Mancarella, H Rudnick. 2016. "Multi-phase assessment and adaptation of power systems resilience to natural hazards". Electric Power Systems Research 136 (2016) 352-361. <https://doi.org/10.1016/j.epsr.2016.03.019>
- Huang, L, X Cun, Y Wang, CS Lai, LL Lai, J Tang, B Zhong. 2018. "Resilience-Constrained Economic Dispatch for Blackout Prevention." IFAC-PapersOnLine 51-28(2018) 450455. <https://doi.org/10.1016/j.ifacol.2018.11.744>
- Jamieson, MR, G Strbac, KRW Bell. 2020. "Quantification and visualisation of extreme wind effects on transmission network outage probability and wind generation output." IET Smart Grid 3-2(2020) 112-122. <https://doi.org/10.1049/iet-stg.2019.0145>
- Kappenman, J. 2010. "Geomagnetic Storms and Their Impacts on the U.S. Power Grid". Metatech. <https://irp.fas.org/eprint/geomag.pdf>
- Karagiannis, GM, ZI Turksezer, L Alfieri, L Feyen, E Krausmann. 2017. "Climate change and critical infrastructure-floods". Floods, EUR 28855 EN, Publications Office of the European Union, Luxembourg 2017. https://www.researchgate.net/publication/322024183_Climate_Change_and_Critical_Infrastructure_-_Floods
- Kim, J, M Kamari, S Lee, Y Ham. 2021. "Large-Scale Visual-Data-Driven Probabilistic Risk Assessment of Utility Poles Regarding the Vulnerability of Power Distribution Infrastructure Systems." Journal of Construction Engineering and Management. <https://ascelibrary.org/doi/10.1061/%28ASCE%29CO.1943-7862.0002153>
- Kim, SW, BG Jeon, DG Hahm, MK Kim. 2019. "Seismic fragility evaluation of the base-isolated nuclear power plant piping system using the failure criterion based on stress-strain". Nuclear Engineering and Technology 51-2(2019) 561-572. <https://doi.org/10.1016/j.net.2018.10.006>
- Kyriazis, P, S Argyroudis. 2014. "Seismic Vulnerability Assessment: Lifelines". Encyclopedia of Earthquake Engineering. Chapter: Seismic Vulnerability Assessment:Lifelines. http://dx.doi.org/10.1007/978-3-642-36197-5_255-1

- Li, Y. 2012. "Assessment of damage risks to residential buildings and cost-benefit of mitigation strategies considering hurricane and earthquake hazards. *Journal of Performance of Constructed Facilities* 26-1(2012).
<https://ascelibrary.org/doi/10.1061/%28ASCE%29CF.1943-5509.0000204>
- Lin, L, J Adams. 2007. "Lessons for the Fragility of Canadian Hydropower Components under Seismic Loading". https://www.earthquakescanada.nrcan.gc.ca/hazard-alea/2007/9CCEE/9CCEE_Lin_Adams_p1186.pdf
- Liu, R, M Xiong, D Tian. 2020. "Relationship between Damage Rate of High-Voltage Electrical Equipment and Instrumental Seismic Intensity". *Advances in Civil Engineering* (2021). Article ID 5104214, 10 pages. <https://doi.org/10.1155/2021/5104214>
- Ma, L, M Khazaali, P Bocchini. 2021. "Component-based fragility analysis of transmission towers subjected to hurricane wind load." *Engineering Structures* 242 (2021) 112586. <https://doi.org/10.1016/j.engstruct.2021.112586>
- Ma, L, P Bocchini, V Christou. 2020. "Fragility models of electrical conductors in power transmission networks subjected to hurricanes." *Structural Safety* 82 (2020) 101890. <https://doi.org/10.1016/j.strusafe.2019.101890>
- Mechtenberg, A, B Mclaughlin, M DiGaetano, A Awodele, L Omeeboh, E Etwalu, L Nanjula, M Musaaazi, M Shrimie. 2020. "Health care during electricity failure: The hidden costs". *Plos ONE* 15-11 (2020). <https://doi.org/10.1371/journal.pone.0235760>
- Mohammad-Amin, A. 2015. "Dynamic behavior of operational wind turbines considering aerodynamic and seismic load interaction." *Doctoral Dissertations*. Paper 2375. https://www.researchgate.net/publication/280025120_Dynamic_behavior_of_operational_wind_turbines_considering_aerodynamic_and_seismic_load_interaction
- Mohammadpour, S, M Hosseini. 2022. "Dispersion reduction of the analyses data for more reliable fragility curves of selected electric substations equipment". *Bulletin of Earthquake Engineering* 20 (2022) 5519-5544. <https://link.springer.com/article/10.1007/s10518-022-01391-2>.
- Nofal, OM, JW Van de Lindt, TQ Do. 2020. "Multi-variate and single-variable flood fragility and loss approaches for buildings" *Reliability Engineering & System Safety* 202 (2020) 106971. <https://doi.org/10.1016/j.ress.2020.106971>
- Oswaldo Martin del Campo, J, A Pozos-Estrada, O Pozos-Estradra. 2020. "Development of fragility curves of land-based wind turbines with tuned mass dampers under cyclone and seismic loading." *Wind Energy* 24-7(2020) 737-753. <https://doi.org/10.1002/we.2600>
- Rezaei, SN, L Chouinard, F Legeron, S Langlois. 2015. "Vulnerability analysis of transmission towers subjected to unbalanced ice loads." *International Conference on Applications of Statistics and Probability in Civil Engineering (ICASP) (12th :2015)*
<https://dx.doi.org/10.14288/1.0076203>
- Salman, AM. 2014. "Age-dependent fragility and life-cycle cost analysis of wood and steel power distribution poles subjected to hurricanes". *Master's Thesis, Michigan Technology*

University.2014

<https://digitalcommons.mtu.edu/cgi/viewcontent.cgi?article=1779&context=etds>

- Sánchez-Muñoz, D, JL Domínguez-García, E Martínez-Gomariz, B Russo, J Stevens, M Pardo. 2020. "Electrical Grid Risk Assessment Against Flooding in Barcelona and Bristol Cities" Sustainability 12- 4(2020) 1527. <https://doi.org/10.3390/su12041527>
- Sang, Y, J Xue, M Sahraei-Ardakani, G Ou, "An Integrated Preventive Operation Framework for Power Systems During Hurricanes," in IEEE Systems Journal, vol. 14, no. 3, pp. 3245-3255, Sept. 2020, doi:10.1109/JSYST.2019.2947672.
<https://ieeexplore.ieee.org/document/8889714>
- Shahzad, U. 2022. "Transient stability risk assessment framework incorporating circuit breaker failure and severe weather." Australian Journal of Electrical and Electronics Engineering <https://doi.org/10.1080/1448837X.2021.2023072>
- Tian, L, X Zhang, X Fu. "Collapse simulations of communication tower subjected to wind loads using dynamic explicit method."2020. Journal of Performance of Constructed Facilities 34-3(2020). <https://ascelibrary.org/doi/abs/10.1061/%28ASCE%29CF.1943-5509.0001434>
- Uralinis, A, IM Shohet. 2022. "Development of Exclusive Seismic Fragility Curves for Critical Infrastructure: An Oil Pumping Station Case Study". Buildings 12-6 (2022) 842. <https://doi.org/10.3390/buildings12060842>
- Veeramany, A, GA Coles, SD Unwin, TB Nguyen, JE Dagle. 2018. "Trial Implementation of a Multihazard Risk Assessment Framework for High-Impact Low-Frequency Power Grid Events". IEEE systems journal, 12-4 (2018).
<https://ieeexplore.ieee.org/stamp/stamp.jsp?tp=&arnumber=8016567>
- Wang, W, JW van de Lindt. 2021. "Quantitative modeling of residential building disaster recovery and effects of pre- and post-event policies." International Journal of Disaster Risk Reduction 59 (2021) 102259. <https://doi.org/10.1016/j.ijdrr.2021.102259>
- Wang, W, JW van de Lindt. 2022. "Quantifying the effect of improved school and residential building codes for tornadoes in community resilience." Resilient Cities and Structures 1-1(2022) 65-79. <https://doi.org/10.1016/j.rcns.2022.04.001>
- Wang, Z, F Yang, Y Wang, Z Fang. 2022. "Study on wind loads of different height transmission towers under downbursts with different parameters." Journals Buildings 12-2(2022) 193. <https://doi.org/10.3390/buildings12020193>
- Watson, EB, AH Etemadi. 2020. "Modeling Electrical Grid Resilience Under Hurricane Wind Conditions With Increased Solar and Wind Power Generation." IEEE Transactions on Power Systems 35-2(2020) pp. 929-937. <https://doi.org/10.1109/TPWRS.2019.2942279>
- Williams, JH, R Paulik, TM Wilson, L Wotherspoon, A Rusdin, GM Pratama. 2020. "Tsunami Fragility Functions for Road and Utility Pole Assets Using Field Survey and Remotely Sensed Data from the 2018 Sulawesi Tsunami, Palu, Indonesia". Pure and Applied Geophysics 177-8 (2020). <https://link.springer.com/article/10.1007/s00024-020-02545-6>

- Wilson, G, TM Wilson, NI Deligne, DM Blake, JW Cole. 2017. "Framework for developing volcanic fragility and vulnerability functions for critical infrastructure". Applied Volcanology 6-14(2017). <https://doi.org/10.1186/s13617-017-0065-6>
- Yoshida, Y, R Matsuhashi. 2013. Estimating Power Outage Costs Based on a Survey of Industrial Customers. Electrical Engineering in Japan 185-4 (2013). <https://onlinelibrary.wiley.com/doi/pdf/10.1002/eej.22306>
- Xue, J, F Mohammadi, X Li, M Sahraei-Ardakani, G Ou, Z Pu. 2020. "Impact of transmission tower-line interaction to the bulk power system during hurricane." Reliability Engineering and System Safety 203 (2020) 107079. <https://doi.org/10.1016/j.res.2020.107079>
- Zekavati, AA, MA Jafari, A Mahmoudi. 2021. "Regional seismic risk assessment method for electric power substations: a case study". Life Cycle Reliability and Safety Engineering. 11 (2022) 105115. <https://link.springer.com/article/10.1007/s41872-021-00178-9>
- Zuo, H, K Bi, H Hao, Y Xin, J Li, C Li. 2020. "Fragility analyses of offshore wind turbines subjected to aerodynamic and sea wave loadings." Renewable Energy 160 (2020) pp. 1269-1282. <https://ideas.repec.org/a/eee/renene/v160y2020icp1269-1282.html>

Pacific Northwest National Laboratory

902 Battelle Boulevard
P.O. Box 999
Richland, WA 99354
1-888-375-PNNL (7665)

www.pnnl.gov